Bull Earthquake Eng
https://doi.org/10.1007/s10518-018-0342-8

ORIGINAL RESEARCH PAPER

Historical intermediate-depth earthquakes in the southern Aegean Sea Benioff zone: modeling their anomalous macroseismic patterns with stochastic ground-motion simulations

Ch. Kkallas[1] · C. B. Papazachos[1] · D. Boore[2] · Ch. Ventouzi[1] · B. N. Margaris[3]

Received: 5 July 2017 / Accepted: 28 February 2018

Abstract We model the macroseismic damage distribution of four important intermediate-depth earthquakes of the southern Aegean Sea subduction zone, namely the destructive 1926 **M** = 7.7 Rhodes and 1935 **M** = 6.9 Crete earthquakes, the unique 1956 **M** = 6.9 Amorgos aftershock (recently proposed to be triggered by a shallow event), and the more recent 2002 **M** = 5.9 Milos earthquake, which all exhibit spatially anomalous macroseismic patterns. Macroseismic data for these events are collected from published macroseismic databases and compared with the spatial distribution of seismic motions obtained from stochastic simulation, converted to macroseismic intensity (Modified Mercalli scale, I_{MM}). For this conversion, we present an updated correlation between macroseismic intensities and peak measures of seismic motions (PGA and PGV) for the intermediate-depth earthquakes of the southern Aegean Sea. Input model parameters for the simulations, such as fault dimensions, stress parameters, and attenuation parameters (e.g. back-arc/along anelastic attenuation) are adopted from previous work performed in the area. Site-effects on the observed seismic motions are approximated using generic transfer functions proposed for the broader Aegean Sea area on the basis of V_{S30} values from topographic slope proxies. The results are in very good agreement with the observed anomalous damage patterns, for which the largest intensities are often observed at distances > 100 km from the earthquake epicenters. We also consider two additional "prediction" but realistic intermediate-depth earthquake scenarios, and model their macroseismic distributions, to assess their expected damage impact in the broader southern Aegean area. The results suggest that intermediate-depth events, especially north of central Crete, have a prominent effect on a wide area of the outer Hellenic arc, with a very important impact on modern

✉ Ch. Kkallas
chkkalla@geo.auth.gr

[1] Geophysical Laboratory, Aristotle University of Thessaloniki, Thessaloniki, Greece

[2] U.S. Geological Survey, Menlo Park, CA, USA

[3] Institute of Engineering Seismology and Earthquake Engineering (EPPO-ITSAK), Thessaloniki, Greece

Published online: 05 March 2018

urban centers along northern Crete coasts (e.g. city of Heraklion), in excellent agreement with the available historical information.

Keywords Stochastic simulation · Historical intermediate-depth earthquakes · Aegean Sea · Macroseismic intensity

1 Introduction

The southern Aegean Sea (Fig. 1) is one of the most seismically active regions of the Eurasian-Africa convergence zone, as well as of the entire Alpine-Himalayan belt. This high seismic activity is mainly associated with the subduction of the Eastern Mediterranean oceanic lithosphere under the Aegean microplate (Papazachos and Comninakis 1971; LePichon and Angelier 1979), resulting in the formation of a well-defined Benioff zone (e.g. Papazachos and Comninakis 1969; Caputo et al. 1970; McKenzie 1970, 1978). The Aegean microplate is moving at an average velocity of ∼ 35–40 mm/year towards the southwest, overriding the nearly stalled (∼ 5 mm/year), Mediterranean-Nubian plate system (Reilinger et al. 1997; Papazachos et al. 1998; Papazachos 1999; McClusky et al. 2000; Ganas and Parsons 2009). The subduction is associated with the well-developed Hellenic volcanic arc (e.g. Fytikas et al. 1985; Francalanci et al. 2005), with the Santorini volcanic center being the most active volcano in this region (e.g. Druitt et al. 1999).

The spatial distribution of the intermediate-depth earthquakes in the southern Aegean Sea subduction delineates a rather amphitheatrically shaped Benioff zone, with focal depths ranging between 50 and 170 km. The slab is descending at an angle of ∼ 15°–30°,

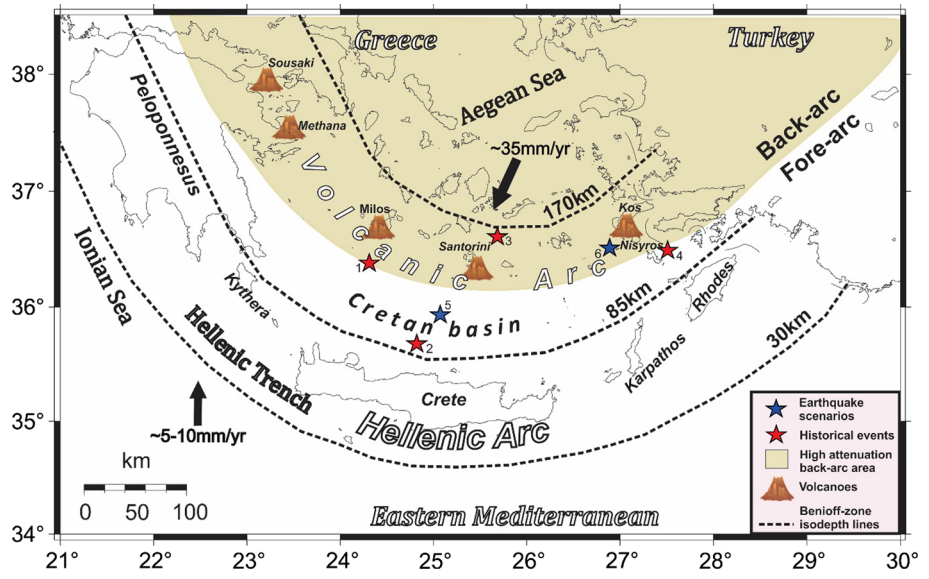

Fig. 1 Schematic geotectonic map of the southern Aegean Sea subduction area. Solid vectors show the Aegean microplate and Eastern Mediterranean plate motions relative to stable Eurasia. The volcanic arc and the Benioff-zone isodepths are also depicted. The shaded area identifies the high-attenuation back-arc area, as proposed by Skarlatoudis et al. (2013) [Sea13 hereinafter]. Historical earthquakes and prediction earthquake scenarios examined in the present work are also shown by red and blue stars, respectively

increasing from west to east, up to the depth of 100 km, becoming steeper ($\sim$ 45°) at larger depths, roughly below the southern Aegean Sea volcanic arc (e.g., Papazachos 1990; Hatzfeld et al. 1993; Knapmeyer 1999; Papazachos et al. 2000). The intermediate-depth earthquakes (h > 50–60 km) under the inner part of the Hellenic arc are mainly strike-slip events, with a significant thrust component, generated by down-dip extension and in-slab compression (e.g. Taymaz et al. 1990; Kiratzi and Papazachos 1995; Benetatos et al. 2004; Kkallas et al. 2013). Shallow earthquakes (h < 50–60 km) in the outer part of arc are generated mainly by thrust (and more rarely strike-slip) faulting, due to an almost horizontal NE–SW compression, from the interaction between the Aegean and eastern Mediterranean lithospheres (e.g. Papazachos and Delibasis 1969; McKenzie 1970, 1978; LePichon and Angelier 1979).

One of the main features of the southern Aegean Sea is its mantle wedge, located beneath the Hellenic volcanic arc (Nisiros–Santorini–Milos–Sousaki–Methana). Due to the presence of low P–S velocities (e.g. Spakman et al. 1993; Spakman 1998; Papazachos et al. 1995; Papazachos and Nolet 1997) and also low Q (high attenuation) values (Ventouzi et al. 2015) in the wedge for the depth range $\sim$ 50–90 km, intense attenuation of P and especially S waves occurs. This strong attenuation pattern is easily recognized in the case of intermediate-depth earthquakes, mainly from the analysis of both macroseismic and ground-motion data (e.g. Papazachos and Comninakis 1969, 1971; Papadopoulos et al. 2002; Boore et al. 2009; Skarlatoudis et al. 2009, 2013). This pattern is very pronounced for several large (M $\sim$ 6.9–7.7) intermediate-depth earthquakes, where anomalous patterns of large macroseismic intensities (I $\geq$ 7–8) have been observed along the fore-arc area, while in back-arc epicentral area (above the hypocenters) the corresponding earthquakes are almost not felt. Similar anomalous back-arc/fore-arc patterns have been observed for a large number of intermediate-depth events recorded in other subduction zones, such as Japan and Tonga (Oliver and Isacks 1967; Kennett and Furumura 2008; Chen et al. 2013; Sun et al. 2014). Strong back-arc/fore arc differences have been also observed in strong motion and macroseismic distributions of intermediate-depth events in the Vrancea subduction (e.g. Sørensen et al. 2010; Vacareanu et al. 2015).

In the present work, we simulate ground motions from several strong historical intermediate depth earthquakes located in the southern Aegean Sea area, for which where only damage information (macroseismic intensities) is available. For the modelling, we employ the stochastic simulation method of Motazedian and Atkinson (2005), as adapted by Boore (2009). More specifically, we compute synthetic seismic motions and convert them to Modified Mercalli macroseismic intensities I_{MM} using an appropriate relationship, proposed in the present work, between peak ground acceleration/velocity (PGA/PGV) and Modified Mercalli Intensity (I_{MM}) value for the intermediate-depth earthquakes of the southern Aegean Sea Benioff zone. We also employ appropriate source and path parameters (e.g. moment magnitude, stress parameter, fault dimensions, high-frequency spectral attenuation, etc.), from previous work on strong-motion simulations and GMPE modeling performed by Kkallas et al. (2018) and Skarlatoudis et al. (2013), hereinafter referenced as Kea18 and Sea13, respectively. Stochastic simulations are developed for four important intermediate-depth earthquakes, namely: (a) Rhodes (June 26, 1926, **M** = 7.7), (b) Crete (February 25, 1935, **M** = 6.9), (c) Milos (May 21, 2002, **M** = 5.9) and, (d) Amorgos (09 July 1956, **M** = 6.9), depicted in Fig. 1 with red stars. Finally, we present "prediction" scenarios for two intermediate-depth earthquakes, located in important source areas of intermediate-depth events, north of Crete (central Hellenic arc) and near the islands of Kos and Nisyros (eastern Hellenic arc), noted with blue stars in Fig. 1.

1.1 Macroseismic intensity and PGA-PGV correlation for intermediate-depth events

Attempts to correlate macroseismic intensities with quantitative measures of recorded ground motion values (e.g. PGA, PGV) have been performed by several researchers for the broader Aegean Sea area (e.g. Theodulidis and Papazachos 1992; Koliopoulos et al. 1998; Tselentis and Danciu 2008), using exclusively shallow earthquake data (typically $h < 50$ km). No such relationships have been proposed for intermediate-depth earthquakes, mainly due to the limited data available. In the present work, we collected all available macroseismic and ground motion data for intermediate-depth events (Table 1) and used them to evaluate the available regional relations, as well as relations usually employed for similar comparisons in California (Wald et al. 1999) for shallow earthquakes. Initially, we collected all available macroseismic Intensity Data Points (IDP) reported in the I_{MM} scale (as employed in Greece) at epicentral distances up to 30 km from recording stations (velocity broadband and accelerographs). We mainly focused on IDP data reported for the same geological formation as the recording PGA–PGV site, in an attempt to establish a reliable correlation between macroseismic intensities and instrumental recordings, without introducing an additional bias due to site-effects. In most cases I_{MM} values were available for the recording site or for sites with similar geology in its immediate vicinity (< 5–10 km). For the few cases, when such I_{MM} values were not available, the collected macroseismic data were spatially interpolated at the site for which an instrumental record was observed, using only sites for which I_{MM} observations at similar geology were available. For these few cases, we did not consider the macroseismic intensity attenuation with distance since the number of IDP within 30 km of each PGA/PGV site was usually quite large, allowing a reliable interpolation. Moreover, as shown by Kea18, attenuation for intermediate-depth events is very different compared to shallow events, since moving away from the epicenter often means that ground motions may actually increase. Using this case-by-case approach, a reliable, average intensity value was assigned to each site for which ground motion measures (PGA and PGV) were observed, if original IDP values at the same site were not reported.

The I_{MM} values for the events in Table 1 do not exceed $I_{MM} = 6$, yet we wish to estimate PGA and PGV for Greek earthquakes for which I_{MM} reaches values often larger than 6. For this reason, we chose to use the well-established relations by Wald et al. (1999).

Table 1 Intermediate-depth earthquakes of the southern Aegean Sea subduction for which macroseismic intensities and PGA/PGV values were collected

ID	Origin time (yyy/mm/dd hh:mm)	Latitude	Longitude	Depth (km)	M*	CR**	Records used (PGA/PGV)
1	1994/05/23 06:46	35.5409	24.6968	68	6.1	0	3/3
2	2004/04/11 06:22	35.9633	23.1454	70	5.2	0	1/1
3	2006/08/01 11:34	36.1853	23.4037	67	6.7	0	27/26
4	2008/03/28 00:16	34.7922	25.3423	49	5.6	1	1/1
5	2008/06/01 05:14	37.2569	22.7037	84	6.2	0	8/8
6	2008/07/15 03:26	35.8500	27.9200	56	6.4	1	7/7

* *M* moment magnitude

** *CR* 0 for in-slab events and 1 for interface events

These relations, however, needed to be adjusted for a bias observed in the Greek I_{MM} values. More, specifically I_{MM} values published for the area of Greece are systematically higher than the corresponding ones employed for the US by $\sim$ 0.5 intensity unit. This bias was originally identified by Shebalin et al. (1974) between the Greek I_{MM} and the MSK and MCS macroseismic scales, and was later confirmed by Papazachos and Papaioannou (1997, 1998) using cross-border macroseismic IDP comparisons between Greece and neighboring Balkan countries (Eq. 1). Moreover, several researchers (e.g. Musson et al. 2009) have shown that the classical modified Mercalli scale [denoted here as I_{MM56}, as suggested by Richter (1958), who completely revised it] and its later modifications (also employed by Wald et al. 1999), and the MCS/MSK scales employed mainly in Europe are practically equivalent (Eq. 2). These observations suggest that a $-$ 0.5 intensity unit correction should be applied to Greek I_{MM} values (Eq. 3), to render them equivalent with the I_{MM56} values used by Wald et al. (1999).

$$I_{MCS/MSK} = I_{MM}^{Greek} - 0.5 \tag{1}$$

$$I_{MM_{56}} = I_{MCS/MSK} \tag{2}$$

$$I_{MM_{56}} = I_{MM}^{Greek} - 0.5 \tag{3}$$

While this average bias of the Greek I_{MM} scale proposed by Eq. (3) may seem rather arbitrary, it is strongly supported by the comparison of all published regional (Greek) I_{MM}^{Greek} and PGA–PGV relations with the corresponding relations from Wald et al. (1999), shown in Fig. 2. The original Wald et al. (1999) relations overestimate PGA and PGV levels when using the reported I_{MM}^{Greek} values, for almost the entire macroseismic scale range considered. If we adjust the Wald et al. (1999) original relations "upwards" by 0.5 units (the bias proposed by Eq. 3), an improved correlation of the "adapted" (to I_{MM}^{Greek}) Wald et al. (1999) relations (red lines in Fig. 2) and the regional (Greek) relations can be observed. It is

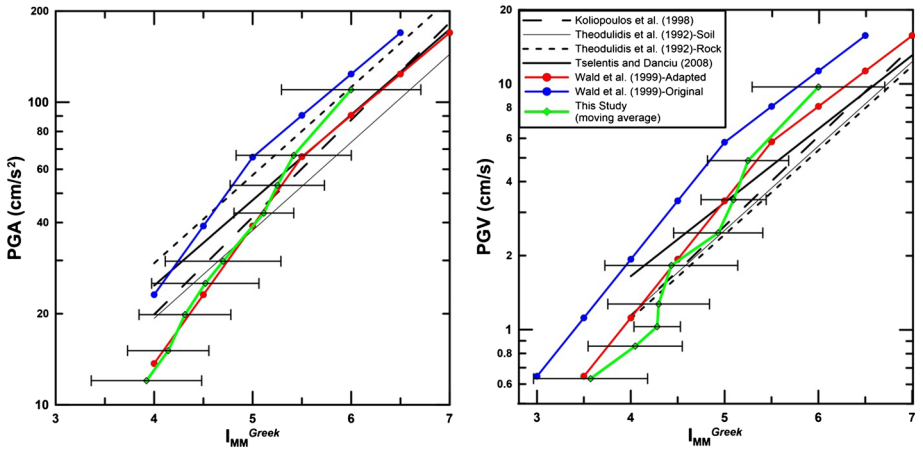

Fig. 2 Comparison of published I_{MM}^{Greek}-PGA (left) and I_{MM}^{Greek}-PGV (right) conversion regional relations for shallow earthquakes in Greece (Theodulidis and Papazachos 1992; Koliopoulos et al. 1998; Tselentis and Danciu 2008), with the original and adapted (to the Greek I_{MM} scale) Wald et al. (1999) relations for California. The moving average of the observed I_{MM} and PGA/PGV data for intermediate-depth earthquakes of the southern Aegean Sea (collected in this work), as well as its standard error (based on the original data variability), are also depicted (see text for explanation)

interesting to observe the somewhat higher ground motions levels (especially PGA) predicted for I_{MM}^{Greek} values $\sim$ 4.0–4.5 in comparison to the adapted Wald et al. (1999) relations. This bias is most probably the combined result of two factors: (a) The imposed linear form of the relation between ln(PGA-PGV) and I_{MM}^{Greek} used in all regional relations, not present in the work of Wald et al. (1999) and, (b) the poor handling of the effective cut-off of smaller PGA or PGV values derived from older trigger-based accelerographs, something usually considered in GMPE studies (e.g. Joyner and Boore 1981; Fukushima and Tanaka 1990). The lack of small PGA or PGV values due to this cut-off resulted in an additional systematic increase of the PGA/PGV values predicted by all regional (Greek) I_{MM}-PGA/PGV relations for small I_{MM}^{Greek}.

In Fig. 2 we also present the I_{MM} values and their corresponding PGA and PGV values for the southern Aegean intermediate-depth earthquake data for the events of Table 1. To overcome the effect of the previously described low PGA–PGV cut-off, we present moving average results (green lines) and their standard error for fixed PGA/PGV intervals, with a 50% overlapping. While the presented results show small-scale variations, and the corresponding MMI values only reach up to values of $I_{MM}^{Greek} \sim 6.0$, we can consider the "adapted" conversion relation of Wald et al. (1999) as quite representative for the intermediate-depth southern Aegean Sea dataset. It should be noted that the I_{MM}^{Greek} bias was observed for the whole range of the Greek I_{MM} scale by Shebalin et al. (1974), while the data used here (Table 1) cover a rather wide depth range (49–84 km), hence any depth-magnitude effects on this bias should not be significant. Therefore, the following adjusted Eqs. (4, 5, adapted from Wald et al. 1999) were used for the conversion of PGA and PGV values to I_{MM}^{Greek} for intermediate-depth earthquakes in the southern Aegean Sea region, and the median I_{MM}^{Greek} value was used in all cases:

$$I_{MM^{Greek}} = \begin{cases} 2.10 * log_{10}\left(\frac{PGV}{5.8}\right) + 5.5, & if \quad 0.37 \le PGV\left(\frac{cm}{s}\right) < 5.8 \\ 3.47 * log_{10}\left(\frac{PGV}{5.8}\right) + 5.5, & if \quad PGV\left(\frac{cm}{s}\right) \ge 5.8 \end{cases} \quad (\sigma = 0.52) \quad (4)$$

$$I_{MM^{Greek}} = \begin{cases} 2.20 * log_{10}\left(\frac{PGA}{66}\right) + 5.5, & if \quad 4.8 \le PGA\left(\frac{cm}{s^2}\right) < 66 \\ 3.66 * log_{10}\left(\frac{PGA}{66}\right) + 5.5, & if \quad PGA\left(\frac{cm}{s^2}\right) \ge 66 \end{cases} \quad (\sigma = 0.44) \quad (5)$$

The reported standard deviations in Eqs. (4) and (5) have been computed from the available Greek I_{MM} and PGA–PGV data for intermediate-depth events. It should be noted that while the data presented in Fig. 2 do not exceed the value $I_{MM} = 6$, we later employ Eqs. (4) and (5) to model intensities up to $I_{MM} \sim 10$. The original Wald et al. (1999) relation employed I_{MM} between 2.5 and 9, as well as PGA and PGV spanning a very large range ($\sim$ 0.005–1.2 g and 0.5–200 cm/s, respectively), hence its applicability for large ground motions is well established. As presented later, the performed simulations adequately model both moderate and large I_{MM} values, without showing a systematic bias/deviation for large I_{MM} values. This is a strong indication that the Wald et al. (1999) relation for intermediate-depth events, once the (known and independently verified) bias of the Greek I_{MM} is considered, is expected to perform equally well for the upper I_{MM} range (7–10).

1.2 Ground—motion modeling

As mentioned earlier, to simulate the examined historical events we used the EXSIM_DMB code by Boore (2009), who modified the original approach of Motazedian and Atkinson (2005). For the stochastic simulation modeling parameters, we followed the approach developed in our previous work (Kea18), where we used the anelastic attenuation from the GMPE modeling developed by Sea13 to constrain the different attenuation patterns and properties for the back-arc and fore-arc area. Figure 3 presents the conceptual model of Sea13 and Kea18, showing a schematic presentation of a cross-section of the Hellenic-arc subduction, with the high Q_S–V_S eastern Mediterranean slab subducting under the Aegean lithosphere, developing a low Q_S (high attenuation) mantle wedge under the volcanic arc. As a result, waves from deep historical events (h: 100–160 km), such as the 1956/07/09 Amorgos aftershock discussed later, are strongly attenuated in the back-arc area (north of the Crete basin, see Fig. 1). On the contrary, waves propagating along the high-Q_S subducting slab result in significant damage at large epicentral distances along the fore-arc islands (Crete and Rhodes), in comparison to back-arc stations at shorter epicentral distances. For shallower events (h: 60–100 km), such as the 1935/02/25 event (north of Crete), the ground motion differences (due to propagation through the attenuating wedge and along the slab) appear only at larger epicentral distances. At short epicentral distances

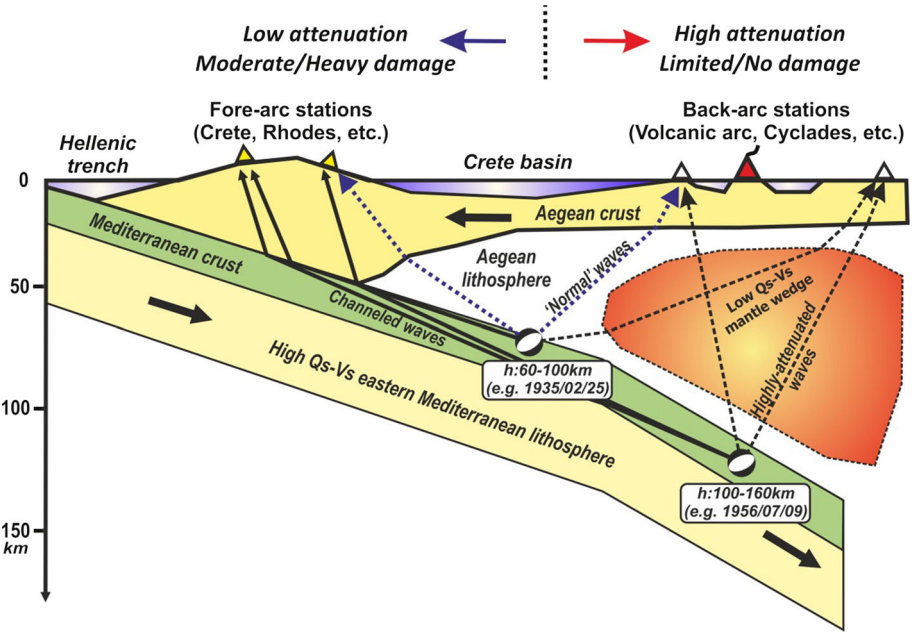

Fig. 3 Schematic arc-normal cross-section of the Hellenic arc subduction, depicting seismic wave propagation for intermediate-depth events (adapted from Sea13 and Kea18). Seismic rays from in-slab events travelling through the low Q_S–V_S back-arc mantle wedge or the high Q_S–V_S subducting eastern Mediterranean slab are depicted by dashed and solid lines, respectively. Seismic energy from deep events (h $\geq$ 100 km) is strongly attenuated in the back-arc area and channeled through the slab, resulting in larger damage in the fore-arc region than in the epicentral area (back-arc area) above the slab. For shallower events (h: 60–100 km) this pattern is prominent only at large distances, since short-distance propagation is not affected by the mantle wedge presence (blue dotted rays).Vertical projections of typical fault-plane solutions are also shown

their propagation paths travel through "normal" lithosphere (dotted rays in Fig. 3). A similar modeling approach was adopted by Vacareanu et al. (2015) to describe back-arc/fore-arc ground motion differences for the Vrancea region.

This depth-distance dependence of anelastic attenuation and slab amplification effects was quantified using ground-motion recordings by Sea13 and adapted in stochastic simulation modeling by Kea18. More specifically, ground-motion simulations for each earthquake included additional spectral attenuation or amplification values for all back-arc and fore-arc stations, depending on the earthquake focal depth. These additional anelastic attenuation/slab amplification effects were introduced by appropriate frequency dependent attenuation/amplification values, proposed by Sea13 for 3 depth ranges (< 80, 80–100, > 100 km), through the EXSIM_DMB "crustal amplification" file. As this scheme depends both on the hypocenter and station locations, custom spectral amplification files need to be created for each event-recording station pair and independent EXSIM_DMB runs need to be performed. Finally, median I_{MM}^{Greek} values were computed from the PGA and PGV values of each simulation (EXSIM_DMB run) using the adjusted Wald et al. (1999) relations.

To include the contribution of site-effects on the simulated macroseismic intensities, we used the generic site amplification functions for NEHRP site condition A/B after the work of Margaris and Boore (1998), while site amplification functions for C and D site conditions were adopted from the work of Klimis et al. (1999, 2006). These transfer functions were adjusted for the crust-mantle density and V_S contrast following Boore et al. (2009), using a local 1D regional velocity model derived from the 3D-model of Papazachos and Nolet (1997). While generic transfer functions cannot capture the detailed local site effects on the predicted ground motions and I_{MM} values, they provide a simple, fast but also efficient way to assess the site conditions in a semi-quantitative manner. Such an approach is clearly appropriate for large scale studies, such as shake maps and macroseismic distribution modeling, and it has also been demonstrated to be effective for more local-scale studies (e.g. Roumelioti et al. 2017). The use of generic site amplifications will inevitably result in local discrepancies, however, as the amplification of certain sites (e.g. deep basin deposits) cannot be adequately described by a generic site-amplification method.

The adopted approach requires that the soil class for each IDP is known. For this reason, we used the SRTM3 topographic model and assigned Vs_{30} values from slope proxies, following Wald and Allen (2007), which has been shown to perform adequately for active regions like the study area (e.g. Lemoine et al. 2012). Furthermore, this approach has been shown to be also appropriate for V_{S30} assessment from slope data for the broader Greece area (Stewart et al., 2014). Using the slope-derived Vs_{30} values, soil classes according to NEHRP (1994) have been assigned to each site for which simulations were performed, since generic transfer functions have not been proposed for Eurocode 8 (EN1998-4) soil classes in the Aegean area. While Vs_{30} assessment from slope proxies is rather approximate, it is suitable for large-scale simulations, as also shown for the area of Greece (e.g. Papazachos et al. 2016).

For the distance-independent high-frequency attenuation (κ_0 values) we employed the results presented by Kea18, who obtained a zero distance kappa estimate, κ_0, assuming a simple linear hypocentral distance scaling (e.g. Anderson and Hough 1984). These results were based on κ values obtained at bedrock stations of the outer arc, originally determined by Ventouzi et al. (2015) from the analysis of EGELADOS network data (Friederich and Meier 2008), and are not affected by the strong back-arc attenuation (see Figs. 1, 3). It is important to notice that: (a) The proposed κ_0 values show a significant spatial variability along the Hellenic arc, therefore different κ_0 values need to be adopted for each simulation

and, (b) even after distance correction (to account for the effect of the anelastic structure), the final κ_0 values are much larger (0.055–0.103) than the values typically reported for A/B NEHRP bedrock formations for shallow events. For example, a value of $\kappa_0 = 0.035$ was proposed for A/B bedrock formations in Greece from Margaris and Boore (1998) and Margaris and Hatzidimitriou (2002; Fig. 3) using shallow earthquakes, while more recently Ktenidou et al. (2012) obtained κ_0 values between 0.015 and 0.040 for A-class bedrock formations (gneiss/granite) in the Mygdonia basin (N.Greece). This suggests that a significant source contribution component is present in the κ_0 values proposed for intermediate-depth events by Kea18 (e.g. due to near source scatter/attenuation, or special source rupture properties). Large κ_0 values have been also observed for intermediate-depth events in other areas, such as the Vrancea region. Sokolov et al. (2005) obtained large values ($\sim$ 0.07) for several bedrock sites, while Pavel and Vacareanu (2015) also obtained similar (0.06–0.07) large values even for the lower attenuation (outer Vrancea arc) region.

To handle the high κ_0 values observed for bedrock sites, as well as the possible influence of site- effects, we considered the typical κ_0 values proposed for A/B, C and D NEHRP soil formations in Greece (Margaris and Boore 1998; Margaris and Hatzidimitriou 2002; Klimis et al. 1999, 2006) presented in Table 2. For each examined earthquake, the κ_0 value reported by Kea18 for the specific earthquake area was increased for the additional κ_0(C)–κ_0(A/B) and κ_0(D)–κ_0(A/B) difference, when the modelling concerned a site of C or D soil site, respectively. In this way, the average, additional high-frequency attenuation affect due to the local soil conditions was incorporated in the modelling, in addition to the bedrock κ_0 values reported by Kea18 for the southern Aegean Sea area. Notice that any additional anelastic attenuation effects were included by using an appropriate Q factor (frequency-dependent) proposed by Kea18, on the basis of results from Sea13.

A critical parameter to be considered for the stochastic simulation modelling is the stress parameter, $\Delta\sigma$. For its determination, we employed the results of Kea18, as shown in Fig. 4, where we also present (for comparison) the stress parameter values from point-source strong-motion simulations for strong to large magnitude (**M** = 6.0–7.1) intermediate-depth events in the Vrancea subduction zone (Romania) from Sokolov et al. (2005),

Table 2 κ_0 values reported for shallow earthquakes for different soil classes in Greece, and values adopted for the intermediate-depth simulations of the present study using results from Kea18 for outer-arc (fore-arc) bedrock sites

NEHRP class	κ_0	Sources	Employed κ_0 values for intermediate-depth events from Kea18, after correcting for soil class					
	Shallow earthquakes		Rhodes 1926	Crete 1935	Milos 2002	Amorgos 1956	Crete prediction scenario	Kos prediction scenario
A/B	0.035	Margaris and Boore (1998)	0.092	0.053	0.058	0.053	0.053	0.084
C	0.044	Klimis et al. (1999, 2006)	0.101	0.062	0.067	0.062	0.062	0.093
D	0.066	Klimis et al. (1999, 2006)	0.123	0.084	0.089	0.084	0.084	0.115

Values for C and D soil classes were estimated using the corresponding difference for shallow events (see text for explanation)

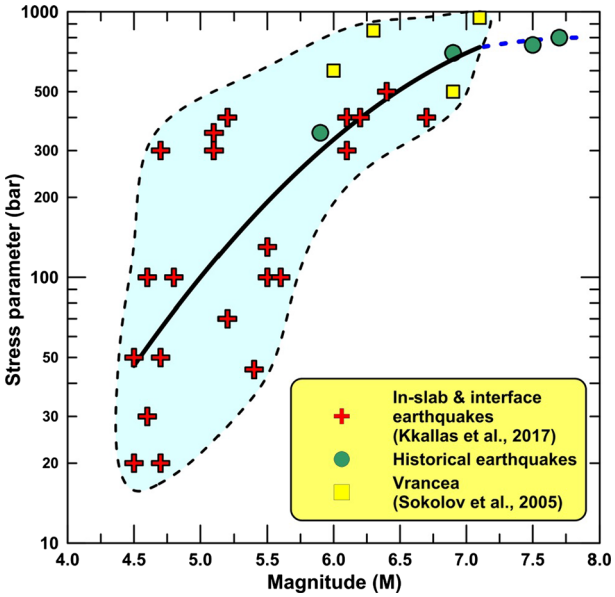

Fig. 4 Stress parameter from stochastic modelling for intermediate-depth earthquakes (in-slab and interface) of the southern Aegean Sea area, versus moment magnitude [red crosses from Kea18, triangles from Sokolov et al. (2005) for the Vrancea subduction area]. The solid and dashed lines depict a smooth 2nd order polynomial data fit and its extrapolation, while the solid circles denote the values adopted for the modelled intermediate-depth events

as observed for the 90–130 km depth range. While stress parameter determinations from ground-motion modelling depend on the specific model and parameters used, Fig. 4 suggests that quite large stress-drop values should be employed for stochastic ground-motion simulations of the considered events. This is in agreement with the results of Gusev et al. (2002) who obtained static stress-drops for Vrancea intermediate-depth events: While static stress-drops are typically much smaller than the stress parameter employed here (which controls the high-frequency spectral levels of the radiated energy), they also showed a significant magnitude dependance of stress-drop values, with a significant increase for events larger than **M** = 7. Since Fig. 4 suggests that stress parameter values between 400 and 700 bar should be used for earthquakes in the range **M** = 6.0–7.1, we employed these values for all simulations, using a slightly larger value (800 bar) for the two (2) largest events considered in this study (**M** $\sim$ 7.7). Due to the large uncertainties observed in Fig. 4, we used rounded values for simplicity, rather than adopting values from the smooth spline polynomial presented in the same Figure. We later examine the effect of the stress parameter variation on the synthetic macroseismic field simulations of the 1926 Rhodes **M** = 7.7 earthquake.

1.3 Simulation of expected ground motions for the historical intermediate-depth events

We simulate ground-motion intensity measures (PGA and PGV) for four well-known intermediate-depth earthquakes which have occurred in the southern Aegean Sea subduction region (Table 3) during the last 100 years, selected on the basis of several criteria.

Table 3 Information on the four (4) historical earthquakes and two (2) predictions scenarios considered in the present study

ID	Origin time (YYYY/MM/DD)	Latitude	Longitude	Depth (km)	M	Strike (o)	Dip (o)	Rake (o)	Length–width* (km)	Stress parameter (bar)	Focal mechanism
1	2002/05/21 20:53 (Milos)	36.3700	24.3100	100	5.9	352	89	4	9.7	350	Benetatos and Kiratzi (2004)
2	1935/02/25 02:51 (Crete)	35.6483	24.8379	80	6.9	50	49	115	28.5	700	Kkallas et al. (2013)
3	1956/07/09 03:24 (Amorgos)	36.6000	25.7000	140	6.9	93	65	35	28.5	700	Brüstle et al. (2014)
4	1926/06/26 19:45 (Rhodes)	36.5000	27.5000	100	7.7	96	83	33	65	800	Kkallas et al. (2013)
5	Earthquake scenario (North of Crete)	35.9380	25.0761	100	7.7	50	59	115	65	800	Kkallas et al. (2013)
6	Earthquake scenario (Nisyros)	36.5000	26.8900	140	7.5	57	89	43	51	750	Kkallas et al. (2013)

*An equal fault length and width was adopted for intermediate-depth events (see Kea18 for details)

The most recent event (2002, **M** = 5.9, Milos island) is the smallest event considered; it occurred at the deeper part of the western segment of the southern Aegean Sea Benioff-zone (h > 100 km). We have included this event in our analysis due to its anomalous macroseismic field pattern (large I_{MM} at large distances, e.g. Crete, and small I_{MM} in the epicentral area in Milos), as well as because it was within the moment magnitude range of the original Kea18 study (**M** = 4.5–6.7) that provides the basis of our modelling. The other three events are large, twentieth century intermediate-depth events (**M** = 6.9–7.7), for which preliminary locations and magnitude estimations were available, including a limited number of instrumental recordings. This allowed us to better constrain their source properties and test the proposed approach, essentially examining the applicability of the Kea18 results to larger magnitudes. Finally, we assess the method application for two (2) prediction scenarios, one similar to a damaging older historical event that occurred north of Crete island and one for the deeper part of the Benioff-zone near the Kos–Nisyros islands, where intense small-magnitude intermediate-depth activity has been systematically observed during the last decades.

Fault-plane solutions for all considered events are listed in Table 3. For the older 1926 (**M** = 7.7) Rhodes earthquake, 1935 (**M** = 6.9) Crete earthquake and the two prediction scenarios, for which fault plane solutions were not available, we adopted typical average focal mechanisms proposed for the event regions by Kkallas et al. (2013). Recent strong events in the same areas, such as the 2016/09/27 **M** = 5.2 intermediate-depth earthquake near Rhodes Island (h = 85 km), showed almost identical fault plane solutions with the average focal mechanism solution adopted here, verifying the reliability of the employed typical solutions.

For the modeling, each fault has to be divided into a specific number of subfaults. The corresponding sub-fault dimensions were calculated from Eq. (6), proposed by Beresnev and Atkinson (1999). Fault dimensions were based on Eq. (7) from Kea18, who proposed equal fault length and width (D in Eq. 7) scaling relations with moment magnitude, using results from Yolsal-Çevikbilen and Taymaz (2012) for southern Aegean Sea intermediate-depth earthquakes.

$$log\Delta l = 0.4M - 2 \tag{6}$$

$$lnD = 1.03M - 3.8 \tag{7}$$

Source velocities were constrained from the regional tomographic model of Papazachos and Nolet (1997) and densities were computed from Brocher (2005) (see also Boore 2016). Figure 5 shows the focal mechanisms of the examined earthquakes and the selected faults used, while in Table 3 the dimensions of the selected faults are listed. A summary of the additional parameters used for our stochastic simulations is given in Table 4.

2 Milos (21 May 2002, M = 5.9)

We first modelled the macroseismic damage of the 2002 Milos island earthquake (21 May 2002, **M** = 5.9, h = 100 km), which is a typical example of a moderate magnitude intermediate-depth earthquake of the southern Aegean Sea. Furthermore, its magnitude falls in the range of the original Sea13 and Kea18 studies, on which we base the present analysis, making this event an excellent first-test candidate. Despite its small magnitude and its large depth (**M** = 5.9, h = 100 km), maximum macroseismic intensities around I_{MM} = IV–V

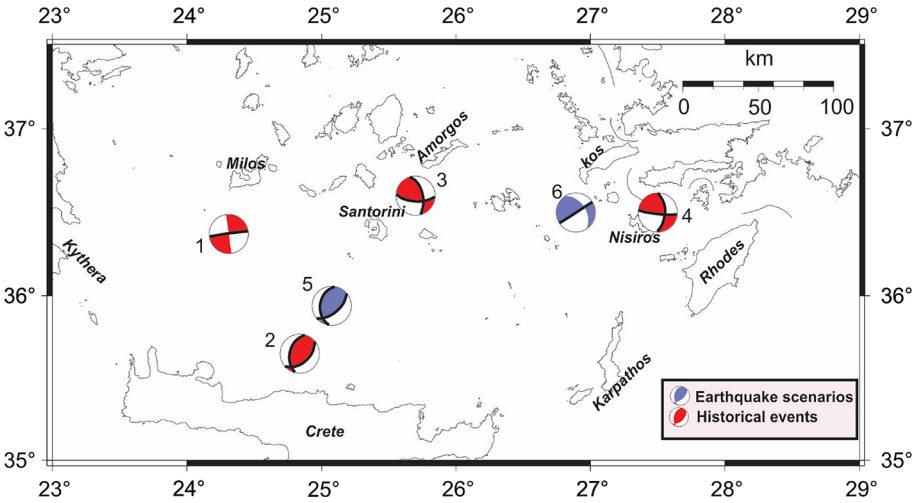

Fig. 5 Focal mechanisms of the four (4) historical and two (2) prediction scenarios of the examined intermediate-depth earthquakes (numbers correspond to the ID column of Table 2, red: historical, blue: prediction scenarios). For each earthquake, the fault plane (one or both) employed for the stochastic simulations are depicted with thick black lines

Table 4 Input parameters of the EXSIM_DMB code, used for the examined southern Aegean Sea intermediate-depth earthquake simulations

Parameters	
Geometric spreading (R^b), b	−1
Q_S model	Kea18
Rupture propagation speed	$0.8V_S$
Subfault source duration	$1/f_0$, where f_0 is the subfault corner frequency
Slip distribution	Uniform slip (random starting point)

were reported in Crete, more than 120 km from its epicenter, with some houses locally damaged (I_{MM} = V–VI) in the city of Heraklion (central Crete), while the earthquake was felt as far away as Egypt.

The simulated macroseismic intensities were obtained from the computed PGA and PGV (RotD50 measure from the two horizontal components, as introduced by Boore 2010) using Eqs. (4), (5). We simulated the intensities at a dense grid of $\sim$ 700 virtual receivers, distributed throughout the broader southern Aegean Sea subduction area. Due to the earthquake's small magnitude (compared to other examined events) and its large depth, the choice of fault plane was not critical for the simulations, an issue discussed later. The selected fault plane is compatible with the preferred intermediate-depth fault orientations proposed by Papazachos (1996), while the adopted stress parameter (350 bars) was based on the distribution presented in Fig. 4.

The spatial variation of simulated macroseismic intensities (I_{MM}) is shown in Fig. 6, while the few originally reported I_{MM} values are also depicted with Latin numbers. A spatially very heterogenous damage pattern is clearly evident for both simulated and

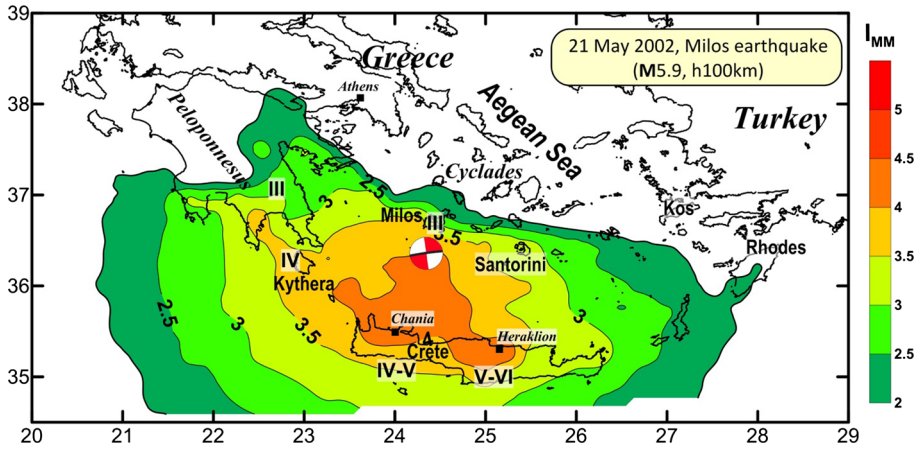

Fig. 6 Spatial distribution of the simulated I_{MM} values for the Milos intermediate-depth earthquake (21 May 2002, **M** = 5.9, h = 100 km). The fault plane used for the simulations is shown with a black solid line. Observed I_{MM} values are also shown with Latin numbers

observed I_{MM} values, with small intensities ($\sim$ 3) predicted (and observed) in the Milos island (epicentral area), as well as in SW Peloponnesus. Larger values are observed near Kythera ($I_{MM} \sim 4$), while peak intensities (I_{MM} = 4–5) are observed and predicted for the island of Crete. The locally larger values observed in the city of Heraklion ($I_{MM} \sim$ 5–6) in central Crete are not seen in the simulated intensities, and are most probably a result of the significant local site-effects (e.g. Savvaidis et al. 2014), not captured by the smooth, generic transfer functions employed here. Large intensities are also predicted for the Chania area, where local damage was also observed (K. Pavlaki, *pers.comm.*). Overall, the reconstructed (simulated) damage pattern adequately describes the observed macroseismic information. Notice that the results also correctly predict the lack of observations in the back-arc area, as the earthquake was not felt in the central Cyclades and Athens.

2.1 Rhodes (26 June 1926, M = 7.7)

The Rhodes earthquake (26 June 1926) is the largest intermediate-depth earthquake instrumentally recorded in the Aegean area and one of the largest in the area's seismic history (Papazachos 1990). The earthquake inflicted heavy damage in the island of Rhodes, as well as neighboring islands (Critikos 1928; Sieberg 1932; Margottini 1982; Ambraseys and Adams 1998; Papazachos and Papazachou 1989, 2003). While macroseismic intensities in the northern part of the Rhodes island varied in the range I_{MM} = 7.5–8.5, in the southern part they increase by at least 0.5 unit, locally exhibiting extreme values for several settlements. A typical example is the town of Archangelos, where 600 houses collapsed, 6 people died and many people were injured (I_{MM} = 11, Papazachos et al. 1997a; Papazachos and Papazachou, 2003). Heavy damage was also sustained in eastern Crete and along the coast of southwestern Turkey. Neighboring islands (Karpathos, Kos) were significantly affected, while in Heraklion (central Crete) many houses collapsed and several people were injured. Extensive damage was also recorded along the broader Asia Minor coastline, while in Alexandria and Cairo eight people were killed. This earthquake was also strongly felt in western and central Crete (Chania, Rethymno, etc.), as well as in the broader eastern and central Mediterranean area (Palestine, Cyprus, Malta, southern

Italy and Albania), with little impact in the back-arc area (low I_{MM}- values), a typical pattern for the largest intermediate-depth events of the Hellenic arc.

While magnitudes between 6.9 and 8.7 in various scales have been assigned to this event, a moment magnitude of **M** = 7.7 was estimated from the average Ms estimate from Karnik (1968) and Ambraseys and Adams (1998), using the conversion relations of Tsampas et al. (2016), which employ a depth correction for **M** estimates from Ms. This estimate is in very good agreement with the m_B = 7.5 computed also by Ambraseys and Adams (1998), which leads to **M** = 7.6–7.7, after conversion to m_b and then to moment magnitude, using the relations of Abe (1981) and Tsampas et al. (2016). The epicenter and depth (h = 100 km) where adopted from Papazachos and Papazachou (2003), in good agreement with the proposed depth (h $\sim$ 110 km) by Ambraseys and Adams (1998) and the local geometry of the Benioff-zone (see Fig. 1). Macroseismic data were collected from the database of Papazachos et al. (1997b). For the simulations, a stress parameter of 800 bars was adopted (see Fig. 4 and earlier discussion). The values of 400 and 1200 bars were also tested (corresponding to a $\pm$ 50% stress parameter change), to quantify its effect, especially for large magnitude events. Since the fault dimensions (length and width $\sim$ 65 km) for this earthquake are comparable to its depth, we have examined the predicted I_{MM} variations for both fault planes. Simulations were performed for all sites for which original macroseismic IDP were available, using again generic transfer functions for site-effect amplifications.

Due to the large number of available observations, we present in Fig. 7 the contoured isoseismals for the observed macroseismic data, as well as the corresponding synthetic (simulated) macroseismic intensity spatial variations for both fault planes. The observed macroseismic field is in good agreement with the simulated values and exhibits strong spatial variations, similar to the Milos earthquake. More specifically, while the earthquake epicenter is located close to the island of Tilos (NW of Rhodes), maximum intensities were observed in southern Rhodes (average I_{MM} = 8.5–9, locally up to 10). The presence of relatively large intensities ($I_{MM} \geq 5$) extends all along the outer Hellenic fore-arc (Karpathos, Crete), to southern Peloponnesus, while being strongly attenuated towards the inner Hellenic arc/Aegean Sea (Cyclades) and the Turkish coast. The observed macroseismic field is nicely reconstructed by the synthetic macroseismic maps, especially the simulation for the N–S trending fault (map L2, Fig. 7c), with similar maximum values in southern Rhodes. The simulations also capture the extended isoseismals along the Hellenic arc, though predicted intensities in western Crete and southern Peloponnesus are still smaller than the observed ones. This suggests that seismic energy has been channeled along the curved subducting eastern Mediterranean lithosphere (see Fig. 1), resulting in larger seismic motions, a pattern that cannot be fully modelled by the proposed approach, which does not account for such strong 3D slab-channeling phenomena.

In Fig. 8a we perform a direct comparison of the I_{MM} values for all sites for which IDP were available, with synthetic values from the best-fit scenario (N–S trending fault plane). In general, the modeled macroseismic intensities capture the main trend of observed damage for a very wide range of values (I_{MM} = 2.5–9.5). While the average bias between observed and predicted MMI values is small ($\sim$ 0.10), the overall RMS is still quite large ($\sim$ 1.1), despite the similarity observed in Fig. 7. While this is partly due to the complicated 3D-wave propagation pattern previously described and site-effects not adequately accounted for by the generic transfer functions, the variability is still significant. To further examine this scatter, we present in Fig. 8a the IDP for the island of Rhodes (red circles) where the largest intensities were observed, since complicated wave propagation/attenuation phenomena are less likely to occur within such a small area. While the observed I_{MM}

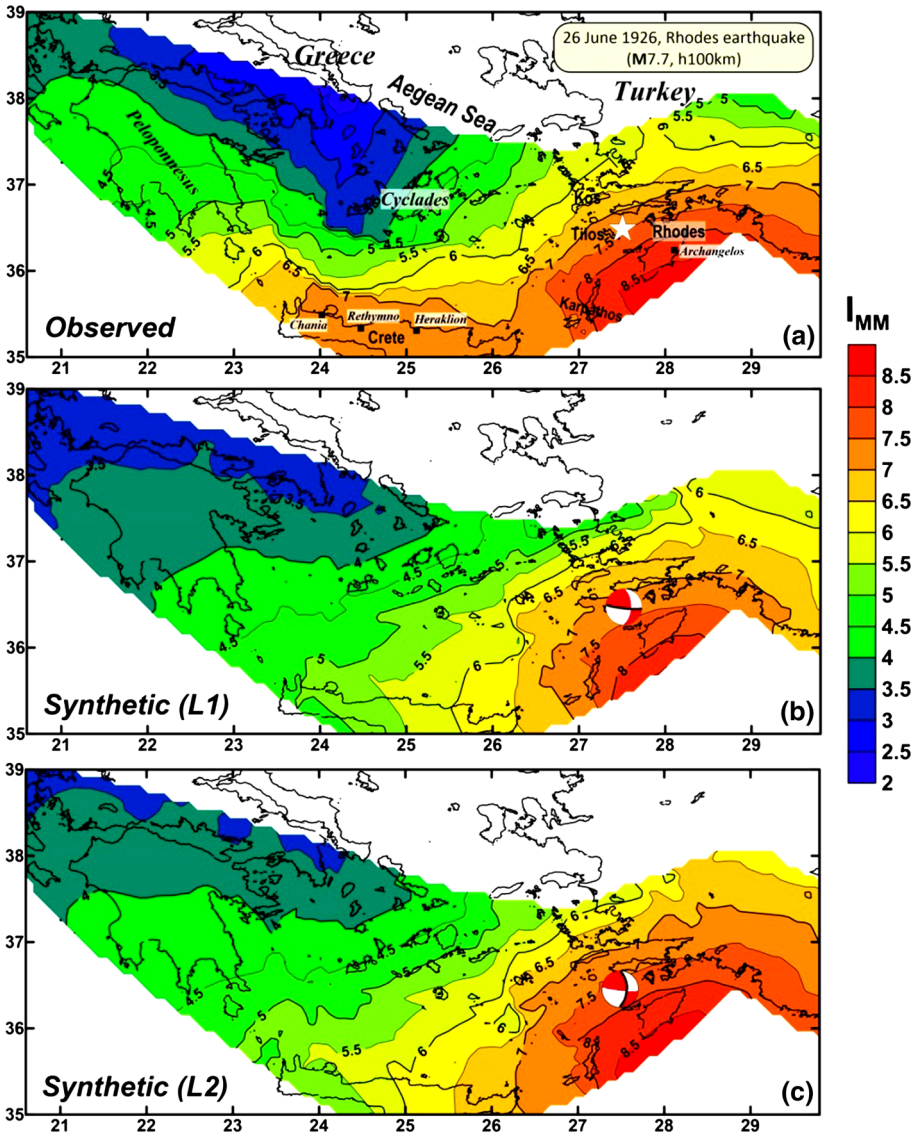

Fig. 7 Spatial distribution of the observed (**a**) and simulated I_{MM} distributions for the two fault planes (**b**, **c**) of the 1926 Rhodes earthquake. The modelled fault planes are depicted in **b**, **c** with a thick solid line

for Rhodes island vary between 7.5 and 11, the corresponding model values span a much smaller range, i.e. 7.0–9.5. However, average intensities for the island of Rhodes are almost identical, namely $\sim$ 8.4 $\pm$ 1.0 and $\sim$ 8.3 $\pm$ 0.7, for observed and predicted I_{MM}, respectively, in agreement with the intensity contours presented in Fig. 7. Although the larger variance of the average observed I_{MM} values (almost twice that of the model predictions) can be due to site effect contributions not accounted for in this work, it is quite probable that some of this variability is also due to the uncertainty involved in the

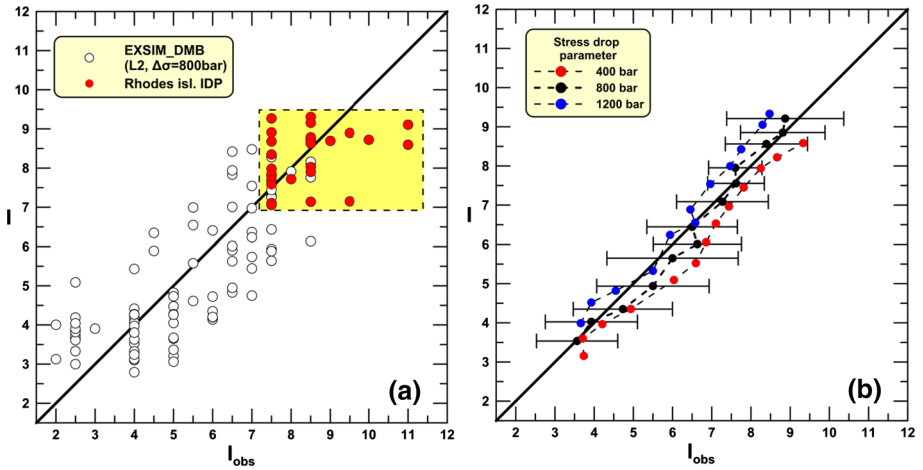

Fig. 8 **a** Comparison of the observed, I_{obs}, against modelled (simulated), I, macroseismic intensities for the 1926, **M**7.7 Rhodes intermediate-depth earthquake (see Figs. 5, 7). Red circles depict macroseismic intensities for the island of Rhodes. **b** Comparison of average (grouped) observed macroseismic intensities for one-unit predicted (modelled) macroseismic intensity intervals (using 50% overlapping). Standard deviations of the observed values are also presented for the employed scenario (stress parameter 800 bar, scenario L2 corresponding to the N–S trending fault plane). Plots for a stress parameter change of ± 50% (400 and 1200 bar) are also plotted for comparison (see text for explanation)

assessment of the macroseismic intensity values, whether this is due to subjective (e.g. erroneous reports) or objective reasons (e.g. differences in building practices).

To further quantify this variability, we present in Fig. 8b a comparison of observed and synthetic intensities, grouped for 1 intensity unit intervals of the predicted (modelled) I_{MM} values, with 50% overlapping. For each bin, the average observed I_{MM} values and its standard deviation are presented. In the same plot, we present the corresponding results for the simulations performed with a smaller (400 bar) and higher (1200 bar) stress parameter (± 50% change). It is clear that while the observed intensity variability with respect to predictions (simulations) is significant (roughly 1 intensity unit), there is a good agreement of the average observed and predicted intensitiesfor the entire data range. Furthermore, the alternative stress parameter synthetics exhibit a rather systematic bias, of the order of ∼ 0.5 intensity units. The results presented in Fig. 8b suggest that the large stress parameter values proposed by Fig. 4, especially the large values used for larger magnitude events (**M** ≥ 7.0) are compatible with the observed damage pattern of this large (**M** = 7.7) earthquake. Furthermore, a ± 50% change of the model stress parameter results in macroseismic intensities which roughly vary by ± 0.5 intensity unit. While this bias is not small, it is at the limit of the data resolution, suggesting that similar stress parameter variations are important but not critical for the modeling.

2.2 Amorgos aftershock (09 July 1956, M = 6.9)

We examined the largest aftershock of the Amorgos 1956 **M** = 7.5 mainshock, the largest twentieth century shallow earthquake in Europe (e.g. Galanopoulos 1981; Comninakis and Papazachos 1986; Makropoulos et al. 1989; Papadopoulos and Pavlides 1992; Ambraseys 2001; Okal et al. 2009). As demonstrated by Brüstle et al. (2014), this was a rare case of dynamic triggering, since the aftershock had an intermediate-depth (∼ 100 km), unlike

the shallow mainshock. While the reported equivalent moment magnitudes for this event ranged between 6.8 and 7.2 (e.g. Galanopoulos 1981; Comninakis and Papazachos 1986; Makropoulos et al. 1989), it had an extremely small, practically negligible impact in the broader focal area, compared to the mainshock which caused extensive damage in the Amorgos–Santorini area. Unpublished reports collected by the authors (C.P.) from Santorini and verbal descriptions from locals verify that the aftershock was felt, but had no impact on the island of Santorini, supporting the suggestion that is is a triggered intermediate-depth event (Brüstle et al. 2014). Moreover, the fault plane solution that the same authors determined was similar to the typical transpressional solutions of deep events in the area (e.g. Taymaz et al. 1990) and clearly different from the mainshock normal faulting. This suggestion is in excellent agreement with earlier relocations (e.g. Makropoulos et al. 1989), as well as the very small Ms = 6.0 magnitude estimated by Ambraseys (2001), which suggests the lack of significant surface waves, compatible with the proposed large depth of the Amorgos aftershock.

To verify the suggested intermediate-depth for this aftershock, we have also modeled its available macroseismic observations. We used the proposed location and equivalent moment magnitude of **M** = 6.9 from Comninakis and Papazachos (1986), obtained from the recordings of the long-period Wiechert seismograph in Athens, in good agreement with previously reported body-wave magnitudes. From the local Benioff-zone geometry (Fig. 1) a depth of 140 km was assigned, while the focal mechanism determined by Brüstle et al. (2014) was used. Though, we considered both fault planes for the simulations, the obtained results were virtually identical, most probably due to the earthquake's relatively large depth, in comparison to its fault dimensions. Finally, a stress parameter of 700 bars was adopted from the event's moment magnitude, based on the distribution of Fig. 4.

Figure 9 presents the spatial distribution of the modeled macroseismic intensities, while observed intensities for Santorini, Anafi and central Crete reported in Modified Mercalli by the Bureau Central International de Sismologie (BCIS 1956) are also presented for comparison. Notice that very few I_{MM} values are available for this event, due to the difficulty in assigning I_{MM} values after the heavy impact of the earlier shallow mainshock. The results confirm the earlier suggestion about the intermediate-depth character of the 1956

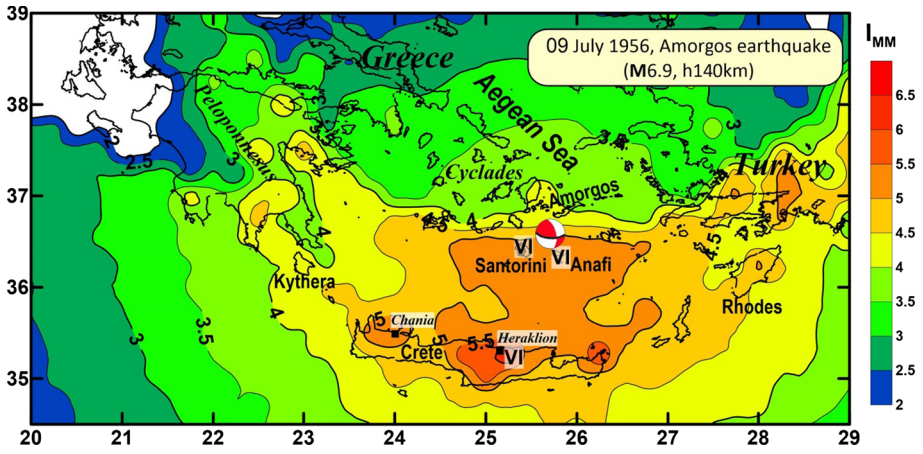

Fig. 9 Spatial distribution of the modelled (simulated) I_{MM} values for the Amorgos aftershock earthquake (09 July 1956, **M** = 6.9, h = 140 km). The fault plane used for the simulation is shown with black solid line, while the reported I_{MM} values (BCIS 1956) are depicted with Latin numbers

aftershock. Maximum synthetic macroseismic intensities are observed near Santorini and Anafi, with large intensities ($I_{MM} \geq 5.5$) extending all the way to northern Crete, in excellent correlation with the available (limited) macroseismic information and verbal reports. If the earthquake was a conventional shallow earthquake, similar to the 1956 mainshock, intensities of the order of $I_{MM} \sim 8.0$ and 3.0–4.0 would have been observed in Santorini–Amorgos islands and northern Crete, respectively. Finally, the obtained results suggest that while events generated in the deeper central part of the Hellenic subduction Benioff zone can have quite large magnitudes (**M** $\sim$ 7.0), their impact in the outer arc (e.g. Crete) is moderate and practically unimportant for the back-arc area.

2.3 Crete (25 February 1935, M = 6.9)

The Crete earthquake (**M** = 6.9) occurred in February 25th, 1935, north of Crete (see Fig. 1). This earthquake is the last one of a sequence of several large (**M** $\sim$ 6.9–7.5) intermediate-depth earthquakes that occurred north of Crete between 1810 and 1935. Due to its large magnitude and proximity to Crete, it resulted in the collapse of many buildings, several deaths and injuries, mainly in city of Heraklion and the villages west of the city (central Crete), also causong damage in the cities of Chania and Rethymno (Papazachos et al. 1997a; Papazachos and Papazachou 2003). The earthquake's magnitude, location and depth were adopted from Papazachos and Papazachou (2003). While the depth (h = 80 km) is in good agreement with the local Benioff-zone geometry presented in Fig. 1, we shifted the epicenter to the east and constrained its location on the major intermediate-depth fault lineament identified by Meier et al. (2004) in this area (Fig. 10). As no information regarding the actual fault characteristics was available, we used the representative fault-plane solution from Kkallas et al. (2013), where both fault planes have similar NW–SE strikes, consistent with the lineament proposed by Meier et al. (2004). We used a stress parameter of 700 bars, similar to the 1956 Amorgos aftershock.

Figure 10 presents a comparison of the spatial distribution of the observed (27 original IDP data, collected from Papazachos et al. 1997b) and the modelled intensities, while a comparison for all available IDP is presented in Fig. 11. Notice that observed I_{MM} values are presented in the form of contours (Fig. 10a) due to their large number, similar to the Rhodes event (Fig. 7). Since the fault dimensions are relatively small (with respect to its depth) and as the 2 fault planes had a similar strike, the simulated I_{MM} values were practically identical; hence results for only for one fault plane are presented in Fig. 10 (scenario L1, NW dipping fault plane). The modelling captures the main features of the observed macroseismic distribution, with larger values in cities of northern Crete (Heraklion, Rethymno, Chania) and southwestern Cyclades islands. Moreover, modelled $I_{MM} = 4.5$ values extend towards the eastern Peloponnesus coastline, in good agreement with observations.

A similar good fit is observed in Fig. 11, where a comparison between the modelled and observed macroseismic intensities is presented for all IDP. The results show a small negative bias ($-$ 0.2 intensity units) between observed and predicted intensities and a larger RMS value ($\sim$ 0.8 intensity units). In the same plot, we also present a comparison between grouped observed and synthetic intensities, similar to Fig. 8b, which verifies the observed $\sim$ 0.2 intensity unit bias. While a smaller stress parameter would predict intensities in better agreement with the pattern observed in Fig. 4, we kept our initial modeling assumptions, due to the much larger overall uncertainty involved in the assessment and modelling of individual macroseismic IDP values.

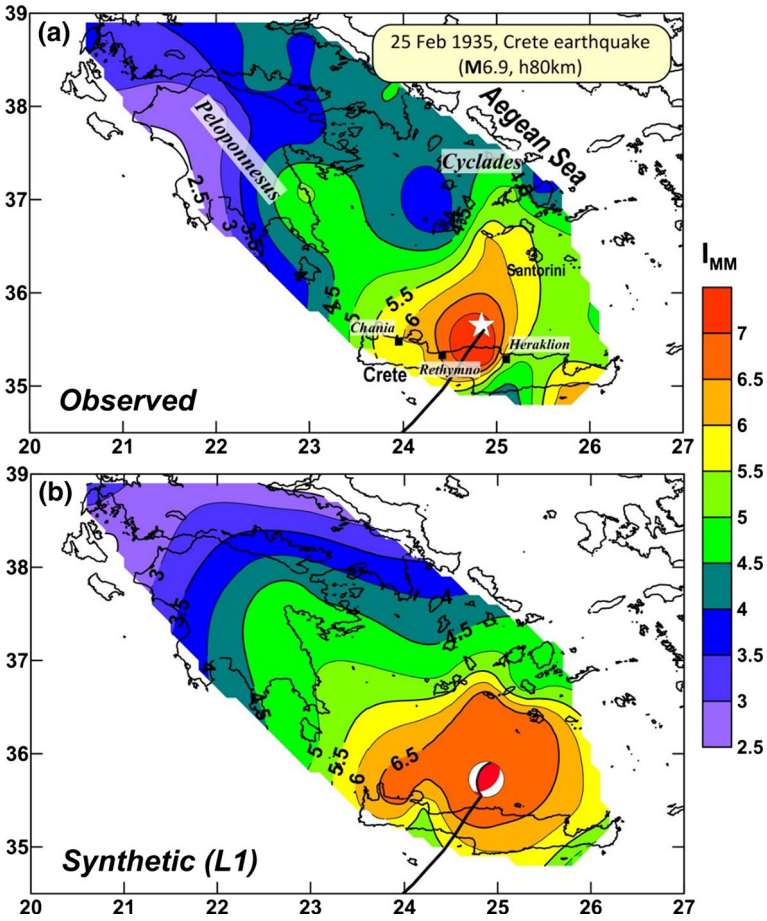

Fig. 10 Spatial distribution of the observed (**a**) and synthetic (**b**) I_{MM} values for the 1935 Crete intermediate-depth earthquake (**M** = 6.9). The fault plane used in the simulations (**b**) and the lineament in the Benioff zone proposed by Meier et al. (2004) are depicted by black solid lines

2.4 Prediction scenarios

To investigate the impact of other large intermediate-depth earthquake scenarios in the southern Aegean Sea area, we present additional results from prediction scenarios performed for two selected subareas. The first prediction scenario concerns the large, intermediate-depth events of the Crete basin (Fig. 1), where several large earthquakes have inflicted heavy damage to urban centers and villages of northern Crete (e.g. Sieberg 1932; Papazachos 1996; Papadopoulos 2011; Ambraseys 2009). Five events with $\mathbf{M} \geq 6.5$ have occurred in this area between 1810 and 1935 (1810, 1856, 1887, 1908, 1935), with the $\mathbf{M} \sim 7.7$, 1856 Crete earthquake (Oct 12, 35.6°N, 25.8°E, see Fig. 12) being the largest one. This earthquake had a significant impact on the whole southern Hellenic arc (Papazachos and Papazachou 1989, 2003; Papadopoulos 2001; Ambraseys 2009), with the heaviest damage occurring in Crete and Rhodes. In Crete, 6512 buildings were heavily damaged and 11,317 were slightly damaged, while for the town of Heraklion almost all

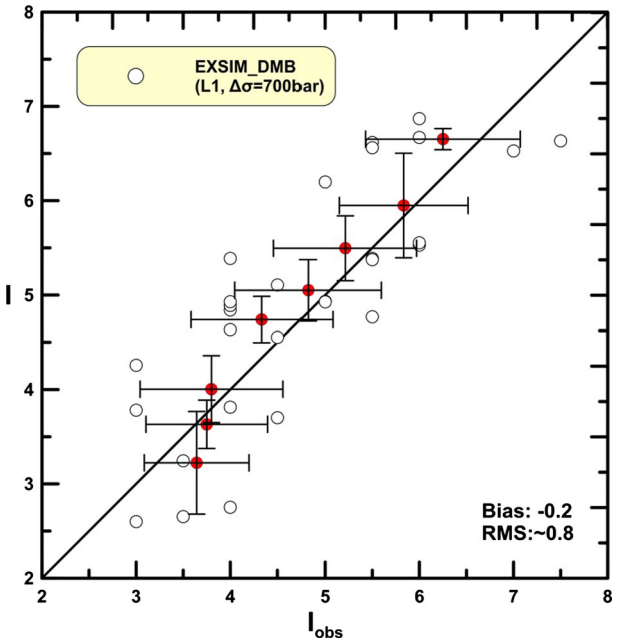

Fig. 11 Comparison of the modelled (synthetic), I, against observed, I_{obs}, macroseismic intensities for the 1935 Crete **M**6.9 intermediate-depth earthquake (open circles). Average (grouped) observed macroseismic intensities (one intensity unit synthetic intensity intervals with 50% overlapping, as in Fig. 8b) are also presented with red circles, together with their one-standard deviation error bars

buildings collapsed or were critically damaged. In total, 538 people died and 637 were injured (Papazachos and Papazachou 2003). While limited information is available for older historical intermediate-depth events in this area, the same damage pattern is recognized in the available historical information.

For our scenario, we simulated the possible impact of a large (**M** = 7.7) earthquake occurring in the Crete basin, similar to the 1856 earthquake. While the damage distribution of the 1856 intermediate-depth event suggests that this event was most probably located in the eastern part of the basin (e.g. Sieberg 1932), we examine here the possible impact of a large intermediate-depth event, located on the fault/lineament identified in the work of Meier et al. (2004), derived on the basis of high-precision locations from temporary seismic networks installed in western and Central Crete. Considering the poor accuracy of historical locations, which are even worse for intermediate-depth earthquakes for which maximum damage is not observed in the epicentral area, we preferred to constrain the earthquake location using existing seismotectonic information. We also adopted for this scenario a magnitude equal to the maximum magnitude historically reported (**M** $\sim$ 7.7) and a depth (h = 100 km) in agreement with the known geometry of the Benioff zone (Fig. 1).

The second test concerns the islands of Kos and Nisyros (Fig. 12) in the eastern, deepest, segment of the southern Aegean Sea Benioff zone. This area is the most seismically active intermediate-depth region of the whole inner Hellenic Arc during the instrumental period (after $\sim$ 1900), with intense small and medium-magnitude intermediate-depth seismicity occurring at depths between 100 and 170 km. Maximum

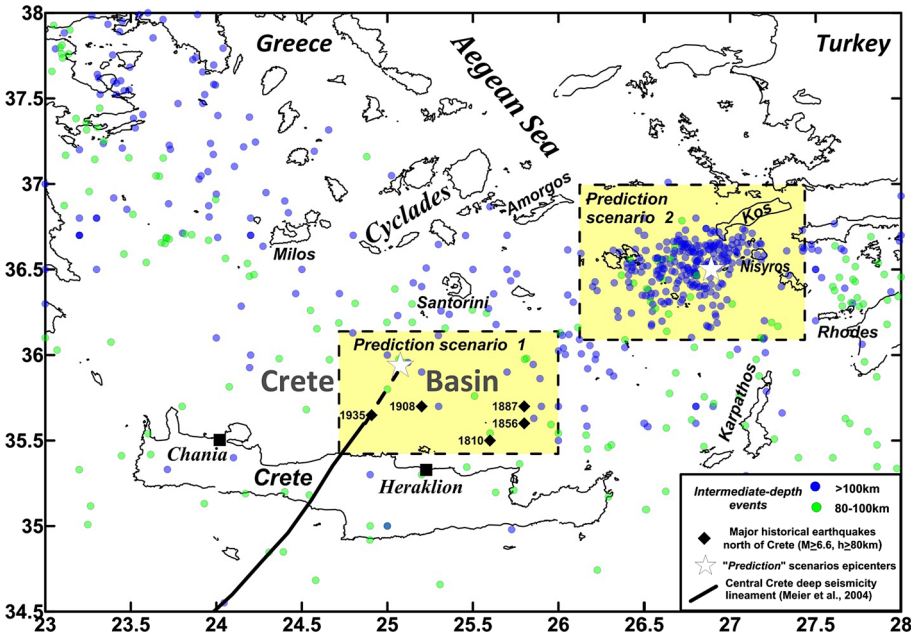

Fig. 12 Intermediate-depth seismicity (Papazachos et al. 2010, available at http://geophysics.geo.auth.gr/) in the southern Aegean area. Prediction scenarios epicenters are denoted with stars. Significant historical intermediate-depth earthquakes north of Crete between 1810 and 1935, as well as the major fault/lineament in the Benioff zone proposed by Meier et al. (2004) are depicted by diamonds and solid line, respectively. The two prediction scenarios areas (central-western Crete basin, Nisyros–Kos deep seismicity cluster) are indicated with yellow boxes

magnitudes of **M** $\sim$ 6.5 are typically considered for this deeper eastern-arc Benioff zone segment, much smaller than the maximum magnitude **M** $\sim$ 8.0 observed along its shallower part (e.g. Papazachos and Papaioannou 1993, Papazachos et al. 2005). However, recent findings show that events up to **M** $\sim$ 7.0 have occurred in the central and western deeper segments of the Hellenic Benioff zone in the twentieth century, such as the 1956 aftershock previously discussed. Since the historical record for these deeper events is clearly incomplete and as the 1926 Rhodes earthquake previously studied had a critical impact on Rhodes, where modern multi-story (often exceeding 10 floors) buildings have been built, we examine here a deeper (h > 100 km) plausible (**M** = 7.5) earthquake scenariofor this deeper Kos–Nisyros seismicity cluster (average depth of 140 km). For both prediction scenarios, the same grid of virtual receivers used for the 2002 Milos earthquake was employed, while all other model parameters (e.g. site-effects) were handled in the same way as for the four (4) events previously examined.

The stochastic simulation approach of the northern Crete **M** = 7.7 earthquake (prediction scenarios 1) was performed for both fault planes of the typical solution proposed by Kkallas et al. (2013) for this area, using a stress parameter of 800 bars (Fig. 4). Despite the large fault dimensions, the simulations (shown in Fig. 13) for both assumed fault planes show similar results, with maximum differences of less than $\sim$ 0.5 intensity units (e.g. Santorini island), possibly due to the similar strike of both fault planes (see also Fig. 5). The results confirm the strongly varying damage pattern of these events, with large intensities (I_{MM} = 8.5–9) estimated for the broader Heraklion area (central Crete).

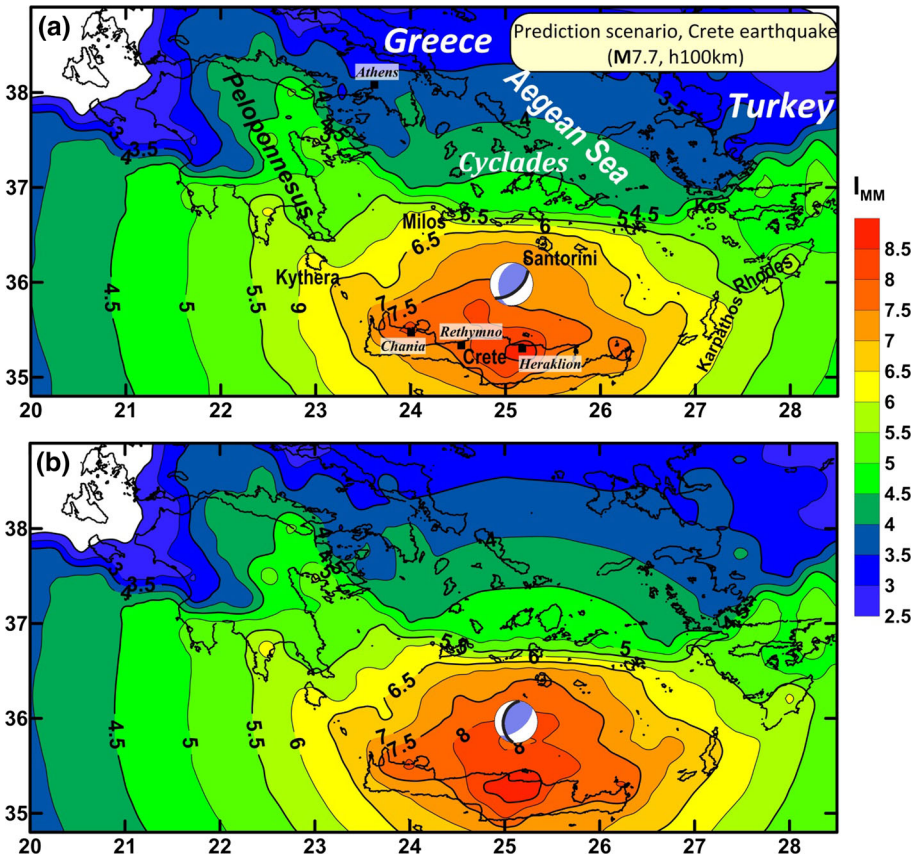

Fig. 13 Expected macroseismic intensity distribution for the first prediction scenario (**M** = 7.7, h = 100 km) north of Crete, considering both fault planes of the typical focal mechanism. The fault plane is depicted in each case with a black solid line on the corresponding fault plane solution. In both cases large intensities ($I_{MM} \geq 7.5$) affect mainly the islands of Crete and Karpathos, with moderate-to-low damage for the adjacent Cyclades islands

Significant damage ($I_{MM} \geq 7.5$) is expected to be observed throughout the whole island of Crete, with I_{MM} values up to 6 extending out to the Kythera, Santorini and Karpathos islands. Again, small macroseismic intensities are predicted for the back-arc area (Athens, Cyclades, etc.), due to the strong back-arc attenuation pattern.

Simulations for the second prediction scenario (**M** = 7.5, h = 140 km, Kos–Nisyros earthquake), which concerns the deeper eastern part of the Benioff-zone, are presented in Fig. 14 for the NE–SW trending fault plane, which is in better agreement with the preferred intermediate-depth fault orientations proposed by Papazachos (1996). It should be noted that the use of the other fault plane led to quite similar results. A strongly varying spatial pattern is again observed, with maximum macroseismic intensities (I_{MM} = 6.5–7) in Rhodes, nearly $\sim$ 120 km away from the earthquake epicenter. For the same distance range, values less than I_{MM} = 4.5 are predicted for the back-arc area (e.g. Amorgos island), verifying the practically non-existent impact of such events in the Cyclades area. Large intensities ($I_{MM} \geq 6$) are also observed for the whole central-eastern outer-arc area, such as central and eastern Crete, Karpathos and the southwestern Turkish coast (Marmaris-Datca

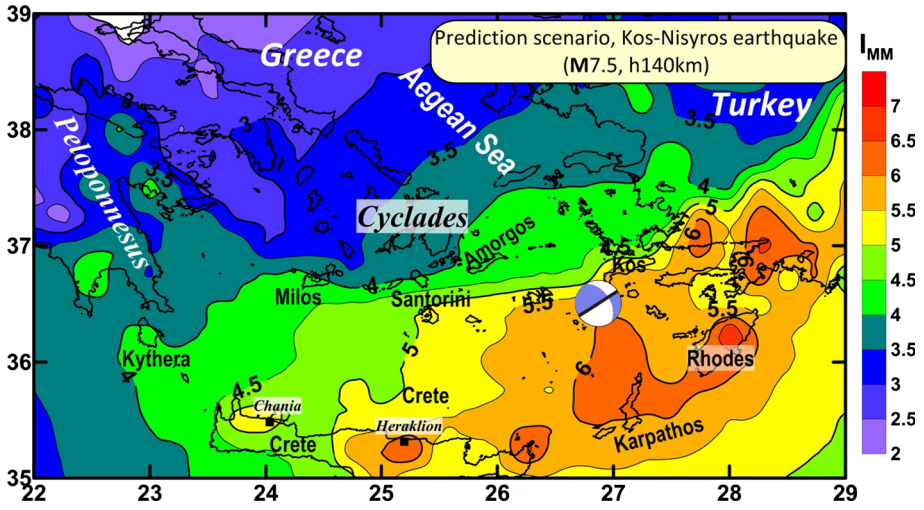

Fig. 14 Expected macroseismic intensity distribution for the second prediction scenario (**M** = 7.5, h = 140 km), concerning the deeper segment of the Benioff zone in the Kos–Nisyros area (eastern Hellenic arc). The examined fault plane is depicted with a black solid line on the corresponding fault plane solution

peninsula), extending to epicentral distances > 200 km. Despite its large magnitude (**M** = 7.5), the predicted damage impact is rather moderate for the whole eastern outer-arc area (Crete–Karpathos–Rhodes-coastal Turkey), clearly due the event's large focal depth, i.e. minimum hypocentral distances starting at $\sim$ 140 km.

3 Conclusions

The simulations performed for four twentieth century moderate-to-large intermediate-depth earthquakes suggest that the stochastic simulation using the EXSIM_DMB code (Boore 2009) and appropriate model parameters from Kkallas et al. (2018) can provide realistic estimates of the past damage distributions for historical intermediate-depth earthquakes of the southern Aegean Sea subduction zone. The stochastic simulations are based on the attenuation model developed by Skarlatoudis et al. (2013), depicted in Fig. 3, which provides the basis for the explanation of the "anomalous" macroseismic intensity pattern observed for such events, where little damage is seen at small epicentral distances (back-arc area), while significant damage is found along the Hellenic fore-arc islands (Crete, Rhodes, Karpathos, etc.) and southern Peloponnesus. Furthermore, the results presented here further verify the original suggestion of Kea18 that relatively large stress-drop values (400–800 bars) need to be employed to adequately simulate large historical earthquake macroseismic data. Despite the large number of parameters necessary for the modelling and the use of simplified generic transfer functions for the incorporation of site-effects, the synthetic macroseismic field captures the main features of the observed damage distribution for the entire magnitude range studied (**M**5.9–7.7). The relation of the Greek version of I_{MM56} against PGA–PGV, adapted from Wald et al. (1999), agrees with earlier results which suggest a systematic bias of the Greek version of the Modified Mercalli scale (Shebalin et al. 1974, Papazachos and Papaioannou 1997, 1998).

In all cases, the high-attenuation back-arc area exhibits small macroseismic intensities as seismic waves cross the low Q region beneath the volcanic arc (Fig. 3), the location of which roughly depicts the southernmost limit of the area where seismic motions are strongly attenuated, as has been observed from the beginning of the twentieth century (Critikos 1928; Sieberg 1932) and adopted in the conceptual model developed by Sea13 and Kea18. On the contrary, maximum macroseismic intensities are observed along the outer Hellenic arc (Crete, Rhodes, etc.), especially for deeper events, quite far from the epicenters of the events (often at distances larger than 120 km). This observation, verified by the simulations, suggests that conventional location methods based on intensity values typically applied for shallow historical events (e.g. Bakun and Wentworth 1997) cannot be readily applied for this type of events.

Events that occur in the shallower part of the Benioff-zone (h $\sim$ 60–100 km) are clearly the main source of seismic hazard from the earthquakes in the Benioff-zone, with intensities reaching values of $I_{MM} \sim 9$ for events with $\mathbf{M} \sim 7.7$, both for the central and the eastern part of the Hellenic Arc. On the contrary, similar large magnitude events (**M**7.0–7.5) within the deeper segment of the Benioff-zone (h $>$ 100 km) have a much smaller maximum damage impact ($I_{MM} \sim$ 6–7). Localized intense damage not predicted from the generic site amplifications used in our simulations may be observed due to site-effects, as also seen in other subduction areas (e.g. Sørensen et al. 2010).

The stochastic simulation of the Amorgos 1956 aftershock suggests that the recent proposal that it is an intermediate-depth event triggered by the 1956 **M** = 7.5 mainshock (Brüstle et al. 2014) is compatible with the synthetic macroseismic intensities and the available macroseismic observations for this aftershock. This observation suggests that dynamic triggering and interaction between shallow and intermediate-depth large magnitude events in the Aegean area is a feasible mechanism, that should be further considered.

The results presented in this study suggest that the role of intermediate-depth earthquakes should be further explored using the employed method as a tool for deterministic seismic hazard assessment of intermediate-depth earthquakes for the southern Aegean Sea area. While at least three $\mathbf{M} \sim$ 7.4–8.0 intermediate-depth events have occurred in the broader Crete basin during the nineteenth century, no such event has been observed during the last $\sim$ 100 years, creating the erroneous impression of seismic safety from such large intermediate-depth events. The 1926 **M** = 7.7 Rhodes earthquake or the first prediction scenario simulations suggest that similar events could have a very wide-area impact, inflicting significant damage throughout the entire central and eastern outer Hellenic arc (Crete, Karpathos, Rhodes). This observation is particularly relevant, if we consider the significant changes in building styles and construction practices adopted during the last 50 years in the southern Aegean Sea area, with modern multi-story buildings now present in many urban centers of the area. Intermediate-depth earthquakes have been proposed to cause some of the archaeological damage to structures built during the Late Minoan IIIB period ($\sim$ 1300–1200 B.C., Jusseret et al. 2013), confirming that these types of earthquakes are a critical factor for seismic hazard assessment for the area of Crete. Similar observations have been made for the Rhodes area, where seventeenth century church repairs indicate the generation of a very strong event in 1717 that affected Rhodes and central Crete and was also felt in eastern Sicily (Stiros et al. 2006). Considering the very large felt area, it is tempting to ascribe this damage to an unknown, large intermediate-depth event.

Except from very large events, such as the 1926 Rhodes earthquake (and to a lesser extent the first prediction scenario considered), the results indicate that the fault plane selection is not critical for reliable macroseismic field simulations. Both these cases, where

the fault plane seems to play a more significant role, have a depth/fault-length ratio smaller than 2 (see Table 3), which seems to be the limit below which the selection of the fault plane is important. In any case, all events with $\mathbf{M} < 7.0$ produce nearly identical damage distributions for both planes, which suggests that alternative tools (e.g. point-source simulations) could be also tested and adapted for such events, allowing rapid but realistic assessments of the ground-motion (and related damage) distributions.

While some details of the damage distribution due to complicated 3D wave propagation phenomena, cannot be captured by the adopted approach (e.g. Rhodes 1926 event) without a major increase in the complexity of the simulations, several aspects of the employed modeling can be easily improved. For example, improved assessment of the site-effects, especially for some of the thick-Neogene deposit basins of Crete, such as the Heraklion (Savvaidis et al. 2014) or the Chania basin (Sarris et al. 2010; Pelekis and Athanasopoulos 2013; Papadopoulos et al. 2017) would allow more realistic simulations of the spatial variability of past macroseismic intensity distributions, hence also for future scenarios.

Acknowledgements We would like to thank Dr. John Douglas and two anonymous reviewers for their constructive and helpful comments, which helped to improve the manuscript. This work has been partly supported by the 3D-SEGMENTS project of the ARISTEIA-I call funded by EC European Social Fund and the Greek Secretariat of Research and Technology. C.P. and M.S. also acknowledge the partial support from the HELPOS (MIS 5002697) project.

Data and resources The intermediate-depth earthquake data used in Fig. 12 are available at http://geophysics.geo.auth.gr/ss/ (last accessed December 2017). The EXSIM_DMB code used for the simulations is available at http://www.daveboore.com/software_online.html (last accessed December 2017). Macroseismic intensities of historical events were collected from the database of macroseismic information for the Aegean area (Papazachos et al. 1997b), available upon request, as well as from the online bulletin of the International Seismological Center (http://www.isc.ac.uk/) and the online archives of the Bureau Central Sismologique Français (http://www.franceseisme.fr/). Broadband velocity-sensor data were collected from permanent Greek seismological networks, operated by the Hellenic Unified Seismological Network (HUSN), available to the public upon request from individual HUSN members. Strong motion data employed in this work were collected from the permanent networks operated by the Institute of Engineering Seismology and Earthquake Engineering (ITSAK) and the National Observatory of Athens, which are also available upon request. Several plots were made using the Generic Mapping Tools version 4 (Wessel and Smith 1998; http://www.soest.hawaii.edu/gmt/, last accessed December 2017).

References

Abe K (1981) Magnitudes of large shallow earthquakes from 1904 to 1980. Phys Earth Plan Inter 27:72–93

Ambraseys NN (2001) Reassessment of earthquakes, 1900–1999, in the Eastern Mediterranean and the Middle East. Geophys J Int 145(2):471–487. https://doi.org/10.1046/j.0956-540X.2001.01396.x

Ambraseys NN (2009) Earthquakes in the Mediterranean and Middle East: a multidisciplinary study of seismicity up to 1900. Cambridge University Press, 968 pp

Ambraseys NN, Adams RD (1998) The Rhodes earthquake of 26 June 1926. J Seismol 2(3):267–292

Anderson JG, Hough SE (1984) A model for the shape of the Fourier amplitude spectrum of acceleration at high frequencies. Bull Seismol Soc Am 74(5):1969–1993

Bakun WU, Wentworth CM (1997) Estimating earthquake location and magnitude from seismic intensity data. Bull Seismol Soc Am 87(6):1502–1521

Benetatos C, Kiratzi A, Papazachos C, Karakaisis G (2004) Focal mechanisms of shallow and intermediate depth earthquakes along the Hellenic Arc. J Geodyn 37(2):253–296

Beresnev IA, Atkinson GM (1999) Generic finite-fault model for ground motion prediction in eastern North America. Bull Seismol Soc Am 89:608–625

Boore DM (2009) Comparing stochastic point-source and finite-source ground-motion simulations: SMSIM and EXSIM. Bull Seismol Soc Am 99(6):3202–3216. https://doi.org/10.1785/0120090056

Boore DM (2010) Orientation-independent, non geometric-mean measures of seismic intensity from two horizontal components of motion. Bull Seismol Soc Am 100:1830–1835

Boore DM (2016) Determining generic velocity and density models for crustal amplification calculations, with an update of the Boore and Joyner (1997) generic site amplification for $$ \bar{V}_{S} (Z) = 760\;{\text{m/s}}. Bull Seismol Soc Am 106:316–320

Boore DM, Skarlatoudis AA, Margaris BN, Papazachos CB, Ventouzi C (2009) Along-arc and back-arc attenuation, site response, and source spectrum for the intermediate-depth 8 January 2006 M 6.7 Kythera, Greece, Earthquake. Bull Seismol Soc Am 99(4):2410–2434. https://doi.org/10.1785/0120080229

Brocher TM (2005) Empirical relations between elastic wavespeeds and density in the Earth's crust. Bull Seismol Soc Am 95(6):2081–2092

Brüstle A, Friederich W, Meier T, Gross C (2014) Focal mechanism and depth of the 1956 Amorgos twin earthquakes from waveform matching of analogue seismograms. Solid Earth 5(2):1027

Bureau Central International de Sismologie (B.C.I.S.): Monthly bulletins, Strasbourg

Caputo M, Panza GF, Postpischl D (1970) Deep structure of the Mediterranean basin. J Geophys Res 75(26):4919–4923

CEN, the European Committee for Standardization (2005) Eurocode 8: Design of structures for earthquake resistance—part 4: Silos, tanks and pipelines. European Standard EN 1998-4, Brussels, Belgium

Chen KH, Kennett BLN, Furumura T (2013) High-frequency waves guided by the subducted plates underneath Taiwan and their association with seismic intensity anomalies. J Geophys Res Solid Earth 118(2):665–680. https://doi.org/10.1002/jgrb.50071

Comninakis P, Papazachos B (1986) A catalogue of earthquakes in Greece and the surrounding area for the period 1901–1985 univ Thessaloniki geophys, Lab. Publ.

Critikos NA (1928) Le tremblement de terre de la mer de Crete du 26 juin 1926; étude macroséismique. Annales Oberv Natl Athenes 10:39–46

Druitt TH, Edwards L, Mellors RM, Pyle DM, Sparks RSJ, Lanphere M, Davies M, Barriero B (1999) Santorini volcano. Geol Soc London Mem, 19:162 pp

Francalanci L, Vougioukalakis G, Perini G, Manetti P (2005) A West–East traverse along the magmatism of the South Aegean volcanic arc in the light of volcanological, chemical and isotope data. Dev Volcanol 7:65–111

Friederich W, Meier T (2008) Temporary seismic broadband network acquired data on hellenic subduction zone. Eos Trans Am Geophys Union 89(40):378. https://doi.org/10.1029/2008EO400002

Fukushima Y, Tanaka T (1990) A new attenuation relation for peak horizontal acceleration of strong earthquake ground motion in Japan. Bull Seismol Soc Am 80:757–778

Fytikas M, Innocenti F, Manetti P, Mazzuoli R, Pecerillo A, Villari L (1985) Tertiary to Quaternary evolution of the volcanism in the Aegean region. In: Dixon JF, Robertson AHF (eds) The geological evolution of the Eastern Mediterranean. Blackwell Publ, Oxford, p 848

Galanopoulos AG (1981) The damaging shocks and the earthquake potential of Greece. Ann Geol Pays Hellen 30:648–724

Ganas A, Parsons T (2009) Three-dimensional model of Hellenic arc deformation and origin of the cretan uplift. J Geophys Res Solid Earth 114:1–14

Gusev A, Radulian M, Rizescu M, Panza GF (2002) Source scaling of intermediate-depth Vrancea earthquakes. Geophys J Int 151(3):879–889

Hatzfeld D, Besnard M, Makropoulos K, Voulgaris N, Kouskouna V, Hatzidimitriou P, Panagiotopoulos D, Karakaisis G, Deschamps A, Lyon-Caen H (1993) Subcrustal microearthquake seismicity and fault plane solutions beneath the Hellenic arc. J Geophys Res Solid Earth 98(B6):9861–9870

Joyner WB, Boore DM (1981) Peak horizontal acceleration and velocity from strong-motion records including records from the 1979 Imperial Valley, California, Earthquake. Bull Seismol Soc Am 71:2011–2038

Jusseret S, Langohr C, Sintubin M (2013) Tracking earthquake archaeological evidence in Late Minoan IIIB (~ 1300–1200 BC) Crete (Greece): a proof of concept. Bull Seismol Soc Am 103(6):3026–3043

Karnik V (1968) Seismicity of the European Area, Parts I and II. Academia-J. Reidel, Praha-Dordrecht, p 1971

Kennett BLN, Furumura T (2008) Stochastic waveguide in the lithosphere: Indonesian subduction zone to Australian craton. Geophys J Int 172(1):363–382. https://doi.org/10.1111/j.1365-246X.2007.03647.x

Kiratzi AA, Papazachos CB (1995) Active deformation of the shallow part of the subducting lithospheric slab in the Southern Aegean. J Geodyn 19:65–78

Kkallas C, Papazachos K, Scordilis E, Margaris V (2013) Re-examining the stress field of the broader Southern Aegean subduction area using an updated focal mechanism database. Bull Geol Soc Greece 47(2):563–573. http://geolib.geo.auth.gr/index.php/bgsg/article/view/10658/10384

Kkallas C, Papazachos CB, Margaris BN, Boore D, Ventouzi C, Skarlatoudis A (2018) Stochastic strong ground motion simulation of the southern Aegean Sea Benioff zone intermediate-depth earthquakes.

Bull Seismol Soc Am. https://pubs.geoscienceworld.org/ssa/bssa/articleabstract/525973/stochastic-strong-ground-motion-simulation-of-the?redirectedFrom=PDF
Klimis NS, Margaris BN, Koliopoulos PK (1999) Site-dependent amplification functions and response spectra in Greece. J Earthq Eng 3(02):237–270
Klimis N, Margaris B, Anastasiadis A, Koliopoulos P, Kirtas Em (2006) Smoothed Hellenic rock site amplification factors. In: 5th Hellenic congress of geotechnical and geoenvironmental engineering, vol 2, pp 239–246, Xanthi, Greece (**in Greek**)
Knapmeyer M (1999) Geometry of the Aegean Benioff zones. Ann Geophys 42(1):29–38
Koliopoulos PK, Margaris BN, Klimis NS (1998) Duration and energy characteristics of Greek strong motion records. J Earthq Eng 2(3):391–417. https://doi.org/10.1080/13632469809350328
Ktenidou O-J, Drouet S, Theodulidis N, Chaljub M, Arnaouti S, Cotton F (2012) Estimation of kappa (κ) for a sedimentary basin in Greece (EUROSEISTEST): Correlation to site characterization parameters. In: Proceedings of 15th world conference of earthquake engineering, Lisbon, Portugal, 24–28 September, 10 pp
Lemoine A, Douglas J, Cotton F (2012) Testing the applicability of correlations between topographic slope and VS30 for Europe. Bull Seismol Soc Am 102(6):2585–2599
LePichon X, Angelier J (1979) The Hellenic arc and trench system: a key to the neotectonic evolution of the eastern Mediterranean area. Tectonophysics 60:1–42
Makropoulos KC, Drakopoulos JK, Latousakis JB (1989) A revised and extended earthquake catalogue for Greece since 1900. Geophys J Int 98(2):391–394
Margaris BN, Boore DM (1998) Determination of $\Delta\sigma$ and $\kappa 0$ from response spectra of large earthquakes in Greece. Bull Seismol Soc Am 88(1):170–182
Margaris BN, Hatzidimitriou PM (2002) Source spectral scaling and stress release estimates using strong-motion records in Greece. Bull Seismol Soc Am 92(3):1040–1059
Margottini G (1982) Osservazioni su alcuni grandi terremoti con epicentro in oriente. Campo macrosismico in Italia del terremoto greco del 1903, Rep. CNEN-RT/AMB(82)3, Comit. Naz. Energ. Nucleare, Rome
McClusky S, Balassanian S, Barka A, Demir C, Ergintav S, Georgiev I, Gurkan O, Hamburger M, Hurst K, Kahle H, Kastens K (2000) Global Positioning System constraints on plate kinematics and dynamics in the eastern Mediterranean and Caucasus. J Geophys Res Solid Earth 105(B3):5695–5719
McKenzie DP (1970) Plate tectonics of the Mediterranean region. Nature 226(5242):239–243. https://doi.org/10.1038/226239a0
McKenzie D (1978) Active tectonics of the Alpine-Himalayan belt: the Aegean Sea and surrounding regions. Geophys J R Astron Soc 55:217–254
Meier T, Dietrich K, Stöckhert B, Harjes HP (2004) One-dimensional models of shear wave velocity for the eastern Mediterranean obtained from the inversion of Rayleigh wave phase velocities and tectonic implications. Geophys J Int 156(1):45–58. https://doi.org/10.1111/j.1365-246X.2004.02121.x
Motazedian D, Atkinson GM (2005) Stochastic finite-fault modeling based on a dynamic corner frequency. Bull Seismol Soc Am 95(3):995–1010. https://doi.org/10.1785/0120030207
Musson RMW, Grünthal G, Stucchi M (2009) The comparison of macroseismic intensity scales. J Seismol 14(2):413–428. https://doi.org/10.1007/s10950-009-9172-0
National Earthquake Hazards Reduction Program (1994) FEMA report 222A: Recommended provisions for seismic regulations for new buildings and other structures, Part 1: provisions. Building Seismic Safety Council, Washington D.C., p 290
Okal EA, Synolakis CE, Uslu B, Kalligeris N, Voukouvalas E (2009) The 1956 earthquake and tsunami in Amorgos, Greece. Geophys J Int 178(3):1533–1554. https://doi.org/10.1111/j.1365-246X.2009.04237.x
Oliver J, Isacks B (1967) Deep earthquake zones, anomalous structures in the upper mantle, and the lithosphere. J Geophys Res 72(16):4259–4275. https://doi.org/10.1029/JZ072i016p04259
Papadopoulos, GA, Ziazia M, Plessa A, Ganas A, Karastathis V, Melis N, Stavrakakis G (2002), Seismic anisotropy in the East Mediterranean Lithosphere: The Mw = 6.3 Karpathos Intermediate Depth Earthquake of 22 January 2002 in the Hellenic Arc. In: XXVII Gen Ass Eur Seism Soc, Genova
Papadopoulos G (2011) A seismic history of Crete. Ocelotos Publ, Athens, p 385
Papadopoulos GA, Pavlides SB (1992) The large 1956 earthquake in the South Aegean: macroseismic field configuration, faulting, and neotectonics of Amorgos Island. Earth Planet Sci Lett 113(3):383–396
Papadopoulos I, Papazachos C, Savvaidis A, Theodoulidis N, Vallianatos F (2017) Seismic microzonation of the broader Chania basin area (Southern Greece) from the joint evaluation of ambient noise and earthquake recordings. Bull Earthq Eng 15(3):861–888
Papazachos BC (1990) Seismicity of the Aegean and surrounding area. Tectonophysics 178:287–308
Papazachos B (1996) Large seismic faults in the Hellenic arc. Ann Geofisica 36(5):891–903

Papazachos CB (1999) Seismological and GPS evidence for the Aegean–Anatolia Interaction. Geophys Res Lett 26(17):2653–2656
Papazachos BC, Comninakis PE (1969) Geophysical features of the Greek island arc and eastern Mediterranean ridge. Com Ren Séances Conf Reunie Madrid 16(16):74–75
Papazachos BC, Comninakis PE (1971) Geophysical and tectonic features of the Aegean arc. Geophys. Res 76:8517–8533
Papazachos BC, Delibasis ND (1969) Tectonic stress field and seismic faulting in the area of Greece. Tectonophysics 7(3):231–255
Papazachos C, Nolet G (1997) P and S deep velocity structure of the Hellenic area obtained by robust nonlinear inversion of travel times. J Geophys Res B Solid Earth 102(B4):8349–8367
Papazachos BC, Papaioannou CA (1993) Long-term earthquake prediction in the Aegean area based on a time and magnitude predictable model. Pure appl Geophys 140(4):593–612
Papazachos C, Papaioannou C (1997) The macroseismic field of the Balkan area. J Seismol 1(2):181–201
Papazachos C, Papaioannou C (1998) Further information on the macroseismic field in the Balkan area. J Seismol 2(4):363–375
Papazachos B, Papazachou K (1989) The earthquakes of Greece—1st edition. Ziti Publ., Thessaloniki, 294 pp (**in Greek**)
Papazachos B, Papazachou K (2003) The earthquakes of Greece—2nd edition. Ziti Publ., Thessaloniki, 273 pp
Papazachos CB, Hatzidimitriou PM, Panagiotopoulos DG, Tsokas GN (1995) Tomography of the crust and upper mantle in southeast Europe. J Geophys Res 12:405–412
Papazachos BC, Papaioannou CA, Papazachos CB, Savaidis AS (1997a) Atlas of isoseismal maps for strong shallow earthquakes in Greece and the surrounding area (426BC-1995), 4
Papazachos BC, Papaioannou Ch, Papazachos CB, Savvaidis AS (1997b) A data bank of macroseismic information for shallow earthquakes in the southern Balkan area (550BC-1995AD). In: 29th IASPEI General Assembly, Thessaloniki, 18–28 August, Abstracts Volume, 372p
Papazachos B, Papadimitriou E, Kiratzi A, Papazachos C, Louvari E (1998) Fault plane solutions in the Aegean Sea and the surrounding area and their tectonic implications. Boll Geof Teor Appl 39(3):199–218
Papazachos BC, Karakostas VG, Papazachos CB, Scordilis EM (2000) The geometry of the Wadati-Benioff zone and lithospheric kinematics in the Hellenic arc. Tectonophysics 319:275–300
Papazachos BC, Dimitriadis ST, Panagiotopoulos DG, Papazachos CB, Papadimitriou EE (2005) Deep structure and active tectonics of the southern Aegean volcanic arc. Dev Volcanol 7:47–64
Papazachos BC, Comninakis PE, Scordilis EM, Karakaisis GF, Papazachos CB (2010). A catalogue of earthquakes in the Mediterranean and surrounding area for the period 1901–2010, Publ. Geophys. Laboratory, University of Thessaloniki
Papazachos G, Papazachos C, Skarlatoudis A, Kkallas H, Lekkas E (2016) Modelling macroseismic observations for historical earthquakes: the cases of the M = 7.0, 1954 Sofades and M = 6.8, 1957 Velestino events (central Greece). J Seismol 20(1):151–165
Pavel F, Vacareanu R (2015) Kappa and regional attenuation for Vrancea (Romania) earthquakes. J Seismol 19:791–799
Pelekis PC, Athanasopoulos GA (2013) Seismic microzonation of Chania, Crete (Greece) based on SASW measurements and non-linear site response analyses. Soil Dyn Earthq Eng 53:145–159
Reilinger RE, McClusky SC, Qral MB, King RW, Toksoz MN, Barka AA, Kinik I, Lenk O, Sanli I (1997) Global positioning system measurements of present-day crustal movements in the Arabia–Africa–Eurasia plate collision zone. J Geophys Res B Solid Earth 102(B5):9983–9999
Richter CF (1958) Elementary seismology. Freeman, San Francisco, p 768
Roumelioti Z, Kiratzi A, Margaris B, Chatzipetros A (2017) Simulation of strong ground motion on near-fault rock outcrop for engineering purposes: the case of the city of Xanthi (northern Greece). Bull Earthq Eng 15(1):25–49
Sarris A, Loupasakis C, Soupios P, Trigkas V, Vallianatos F (2010) Earthquake vulnerability and seismic risk assessment of urban areas in high seismic regions: application to Chania City, Crete Island, Greece. Nat Hazards 54(2):395–412
Savvaidis A, Margaris B, Theodoulidis N, Lekidis V, Karakostas C, Loupasakis C, Rozos D, Soupios P, Mangriotis M, Dikmen U, Tsangaratos P (2014) Geo-Characterization at selected accelerometric stations in Crete (Greece) and comparison of earthquake data recordings with EC8 elastic spectra. Open Geosci 6(1):88–103
Shebalin, NV, Kárnik V, Hadzievski D (1974) Catalogue of earthquakes 1901–1970, and atlas of isoseismal maps. UNDP/UNESCO Balkan Project, Skopje, 3
Sieberg A (1932) Die Erdbeben. In: Gutenberg B (ed) Handbuch der Geophysik 4, 93–94, Berlin

Skarlatoudis AA, Papazachos CB, Margaris BN, Papaioannou C, Ventouzi C, Vamvakaris D, Bruestle A, Meier T, Friederich W, Stavrakakis G, Taymaz T (2009) Combination of acceleration-sensor and broadband velocity-sensor recordings for attenuation studies: the case of the 8 January 2006 Kythera intermediate-depth earthquake. Bull Seismol Soc Am 99(2A):694–704

Skarlatoudis AA, Papazachos CB, Margaris BN, Ventouzi C, Kalogeras I (2013) Ground-motion prediction equations of intermediate-depth earthquakes in the Hellenic arc, Southern Aegean subduction area. Bull Seismol Soc Am 103(3):1952–1968. https://doi.org/10.1785/0120120265

Sokolov V, Bonjer KP, Oncescu M, Rizescu M (2005) Hard rock spectral models for intermediate-depth Vrancea, Romania, earthquakes. Bull Seismol Soc Am 95(5):1749–1765

Sørensen MB, Stromeyer D, Grünthal G (2010) A macroseismic intensity prediction equation for intermediate depth earthquakes in the Vrancea region, Romania. Soil Dyn Earthq Eng 30(11):1268–1278

Spakman W (1998) Upper mantle delay time tomography with an application to the collision zone of the Eurasian, African and Arabian plates. Ph.D. Thesis, Univ. of Utrecht, 53, 200 pp

Spakman W, Van der Lee S, Van der Hilst RD (1993) Travel-time tomography of the European–Mediterranean mantle down to 1400 km. Phys Earth Plant Int 79:3–74

Stewart JP, Klimis N, Savvaidis A, Theodoulidis N, Zargli E, Athanasopoulos G, Pelekis P, Mylonakis G, Margaris B (2014) Compilation of a local VS profile database and its application for inference of VS30 from geologic- and terrain-based proxies. Bull Seismol Soc Am 104(6):2827–2841. https://doi.org/10.1785/0120130331

Stiros S, Papageorgiou S, Kontogianni V, Psimoulis P (2006) Church repair swarms and earthquakes in Rhodes Island, Greece. J Seismol 10(4):527–537

Sun D, Miller MS, Piana Agostinetti N, Asimow PD, Li D (2014) High frequency seismic waves and slab structures beneath Italy, Earth Planet. Sci Lett 391:212–223. https://doi.org/10.1016/j.epsl.2014.01.034

Taymaz T, Jackson J, Westaway R (1990) Earthquake mechanisms in the Hellenic Trench near Crete. Geophys J Int 102(3):695–731

Theodulidis NP, Papazachos BC (1992) Dependence of strong ground motion on magnitude-distance, site geology and macroseismic intensity for shallow earthquakes in Greece: I, peak horizontal acceleration, velocity and displacement. Soil Dyn Earthq Eng 11(7):387–402

Tsampas AD, Scordilis EM, Papazachos CB, Karakaisis GF (2016) Global-magnitude scaling relations for intermediate-depth and deep-focus earthquakes. Bull Seismol Soc Am. https://doi.org/10.1785/0120150201

Tselentis GA, Danciu L (2008) Empirical relationships between modified Mercalli intensity and engineering ground-motion parameters in Greece. Bull Seismol Soc Am 98(4):1863–1875. https://doi.org/10.1785/0120070172

Vacareanu R, Radulian M, Iancovici M, Pavel F, Neagu C (2015) Fore-arc and back-arc ground motion prediction model for Vrancea intermediate depth seismic source. J Earthq Eng 19(3):535–562

Ventouzi C, Papazachos CB, Papaioannou C, Hatzidimitriou P, The EGELADOS Working Group (2015) Qp and Qs attenuation models of the southern Aegean subduction area. Paper presented at 15th European conference on earthquake engineering and 34th General Assembly of the European Seismological Commission, Istanbul, Turkey

Wald DJ, Allen TI (2007) topographic slope as a proxy for seismic site conditions and amplification. Bull Seismol Soc Am 97(5):1379–1395. https://doi.org/10.1785/0120060267

Wald DJ, Quitoriano V, Heaton TH, Kanamori H (1999) Relationships between peak ground acceleration, peak ground velocity, and modified Mercalli intensity in California. Earthq Spectra 15(3):557–564

Wessel P, Smith WH (1998) New, improved version of generic mapping tools released. Eos Trans Am Geophys Union 79(47):579

Yolsal-Çevikbilen S, Taymaz T (2012) Earthquake source parameters along the Hellenic subduction zone and numerical simulations of historical tsunamis in the Eastern Mediterranean. Tectonophysics 536–537:61–100. https://doi.org/10.1016/j.tecto.2012.02.019